이학박사 학위논문

Rf-induced evaporative cooling of ^{87}Rb atoms in magnetic traps toward Bose-Einstein condensation

보즈 아인슈타인 응축을 위해 라디오 주파수 증발로 냉각된 자기 우물안의 루비듐 원자 연구

2012년 8월

서울대학교 대학원

물리·천문학부

염다현

Rf-induced evaporative cooling of ^{87}Rb atoms in magnetic traps toward Bose-Einstein condensation

보즈 아인슈타인 응축을 위해 라디오 주파수 증발로 냉각된 자기 우물안의 루비듐 원자 연구

指導敎授 諸元鎬

이 論文을 理學博士學位論文으로 提出함

2012年 5 月

서울大學校 大學院

物理·天文學部

염 다 현

염다현의 理學博士 學位論文을 認准함

2012年 6 月

委 員 長	안 경 원	印
副委員長	제 원 호	印
委 員	박 건 식	印
委 員	신 용 일	印
委 員	노 흥 렬	印

Rf-induced evaporative cooling of ^{87}Rb atoms in magnetic traps toward Bose-Einstein condensation

by

Dahyun Yum, M.S.

Dissertation

Presented to the Faculty of the Graduate School of

Seoul National University

in Partial Fulfillment

of the Requirements

for the Degree of

Doctor of Philosophy

Seoul National University

August 2012

Abstract

Rf-induced evaporative cooling of ^{87}Rb atoms in magnetic traps toward Bose-Einstein condensation

Dahyun Yum
Department of Physics and Astronomy
The Graduate School
Seoul National University

In the fast few decades, the ultra cold atomic system is one of the hottest topic in physics. Various extraordinary phenomena have been studied and reported in the extreme low temperature systems. In this thesis, the experimental procedure and results of trapping and cooling ^{87}Rb bosonic atoms in variety trapping potentials, that are magneto optical trap(MOT), magnetic spherical quadrupole trap, time-averaged potential(TOP) trap and hybrid trap, are described. Though all the works are designed for achieving the Bose-Einstein condensation, the final goal is failed. However the experimental results and all the knowhow of making ultra cold atomic sample are discussed.

The ^{87}Rb atoms are trapped by the magneto optical trap in the 1st chamber and transferred to 2nd chamber of double MOT vacuum system. Magneto optically trapped 10^9 atoms in the 2nd chamber are loaded in the magnetic spherical quadrupole trap after cMOT and optical pumping stage. The cMOT(compressed MOT) is for increasing the atomic density and locating the

atoms in the magnetic trap center. When the cMOT time was decided, the oscillatory motion of atoms in the magnetic trap was observed and the preliminary results are mentioned. In the optical pumping process, the atomic state is transferred to weak field seeking state($|F = 1, m_f = -1 >$) for trapping magnetically.

The temperature of atoms in the magnetic spherical quadrupole trap are lowered by rf-evaporative cooling technique. The state of hot atoms in the trap is changed to the high field seeking sate by resonant field. The temperature of loaded atoms in the magnetic trap is about $60\mu K$ and it is lowered to $20\mu K$. However the magnetic quadrupole trap have zero magnetic field in the center, the majorana spin flip is occurred and loosing atoms near the center. Thus the time-averaged orbiting potential(TOP) trap and hybrid trap are introduced.

The 1×10^7 atoms are trapped in the TOP trap and cooled by rf-evaporation. And also 1×10^5 atoms are trapped in the hybrid trap after evaporative cooling till 2 MHz in the magnetic quadrupole trap. Even though the temperature of atoms have been not reached to the critical temperature of BEC, the experimental result of the trapping and cooling atoms in various trapping potentials is further step closer the BEC.

Keywords : Rf-induced evaporative cooling, ^{87}Rb, ultra cold atoms, magnetic trap potential

Student number : 2004-30931

초 록

지난 몇 십년 동안 원자물리, 특히 낮은 온도의 원자를 포획하는 시스템은 매우 큰 발전이 있었고, 가장 흥미가 있던 분야 중 하나이다. 우리도 다양한 방법으로 원자를 포획, 온도를 낮추었고, 이 논문에서는 그 동안의 연구들을 정리하였다.

먼저 중성 원자를 포획하는 기본적인 방법이 되는 광 자기 포획 방법을 통해 10^{10} 개의 87 루비듐 원자를 포획하였고, 결맞는 레이저를 이용하여 더 좋은 진공으로 옮겨서 약 10^9의 원자를 재 포획하였다. 그러나 광자기 포획 방법으로는 공명 레이저에 의한 운동량 증가 때문에 낮출 수 있는 온도에 한계가 있어서, 다른 포획, 냉각 방법을 사용해야 한다.

가장 많이 사용하는 방법은 자기장만을 이용한 방법이나, 공명주파수에서 멀리 떨어진 주파수의 레이저를 이용하여 포획하는 방법을 사용한다. 이렇게 포획된 원자는 강제증발 방법을 통해 온도를 더 낮출 수 있게 된다. 자기장으로 포획된 원자는 라디오 주파수 장을 이용하여 포획되지 않는 상태로 전이시켜 강제증발 시키고, 광학적 포획방법을 사용할 경우 레이저의 세기를 줄이는 것으로 포텐셜을 낮추어 온도를 낮출 수 있다.

먼저 자기 사중극 우물에 원자를 포획하여 라디오 주파수 증발법을 이용하여 원자의 온도를 $20\mu K$ 까지 낮출 수 있었다. 그러나 자기 사중극 우물은 중앙에 자기장이 0 이고, 자기장이 없으면 원자의 정렬된 스핀이 바뀌기 때문에 지속적인 포획이 불가능하다. 그래서 시간 평균 회전 우물과 레이저 자기장 복합 우물이라는 방법을 도입하여 원자를 포획하였다. 두 방법 모두

충분한 원자를 포획하는 것에는 성공하였으나 온도를 보즈 아인슈타인 응축까지 낮추는데는 실패하였다. 그러나 이 모든 실험적인 과정과 결과들은 저온 원자 연구에 많은 도움을 줄 수 있는 성과이다.

주요어 : 라디오 주파수 증발 냉각, 루비듐, 극 저온 원자, 자기 우물

학 번 : 2004-30931

Contents

List of Figures

Chapter 1

Introduction

1.1 A Brief History of Cold Atomic Physics

The coldest material that human could have seen in the Earth is maybe the snow which is the solid state of the H_2O formed below the critical temperature of $273K$. The cold material and system had been one of the curious part and now a day the physics in a extremely low temperature systems are one of the interesting part in the nature [1–3]. A brief history of achieving and studying cold atoms or molecule is described here below.

The first clue of making low temperature is the Boyle's and Charles's law [4] for the ideal gas given by $PV = nRT$ or $PV = Nk_BT$, where P is pressure, V is volume, R is the Avogadro constant, k_B is the Boltzmann constant and T is the temperature. If the pressure and the volume are controlled, the temperature also could be changed. The Boyle's law is demonstrated in 1662

by a vacuum pump [5].

The first document of the suggestion of an artificial refrigerator is published in 1756 by William Culle [6] and the modern air conditioner is developed in 1906 by William Carrier. The refrigerator and the air-conditioner are one of the necessaries in the today life.

The physical meaningful achievement of cold temperature is the same with the history of the liquify molecules or atoms, i.e. liquid oxygen Hydrogen and Helium. The first achievement of liquify molecule is SO_2 in 1784 by Gaspard Monge, the melting point is $201K$. The liquid oxygen(1877, Raoul Pictet and Louis Paul Cailletet, melting point is $90.19K$), the liquid hydrogen(1898, James Dewar, $20.28K$) and liquid helium(1908, Heike K. Onnes, $4.2K$) [7] is achieved [8]. However the liquefying gases gives a limitation of the cooling mechanism by controlling pressure and volume.

In 1924 an interesting idea on the statistics of photons was suggested by an Indian physicist S. N. Bose [9]. And Albert Einstein considered a gas of non-interacting and boson below a critical temperature would occupy in the lowest energy and acts like one particle which is called Bose-Einstein condensation [10].

In 1938 Fritz London suggested the connection between the superfluidity of liquid ^4He and Bose-Einstein condensation [11, 12]. The superfluid liquid ^4He is a prototype of Bose-Einstein condensation. However, the strong interactions among the helium atoms reduce the number of atoms in a zero momentum state. For a higher condensation fraction, cooling weak interacting particles is considered but the most gases do not remain gaseous state in the low tempera-

ture.

In 1975, Hänsch and Schawlow and Wineland and Dehmelt proposed the idea of laser cooling. The idea of laser cooling was first demonstrated in 1988 by Steven Chu [13]. An experimental result of the laser cooled atoms below the Doppler limit expected earlier was presented by William D. Phillips in 1988 and that is explained by Claude Cohen-Tannoudji [14]. Steven Chu, W. D. Phillips and C. Cohen-Tannoudji awarded Novel Prize in 1997 for the development of methods to cool and trap atoms with laser light. However the laser cooling has a limitation called recoil limit to lower temperature to realize Bose-Einstein condensates.

The Bose-Einstein condensation of dilute gas of alkali atoms was achieved in 1998. Eric Cornell and Carl Wienmann trapped ^{87}Rb atoms in a TOP trap and lowered the temperature by rf-evaporative cooling [15] and Wolfgang Ketterle used Ioffe-Pritchrd trap for achieving Bose-Einstein condensation of Na atoms [16]. They also awarded the Novel Prize in 2001. The Bose Einstein condensation of alkali atoms are produced by many other species of atoms. In alkali atoms, ^{7}Li [17], ^{41}K [18], Cs [19] and ^{85}Rb [20] are cooled down to the Bose-Einstein Condensation and the Hydrogen atoms [21], metastable Helium [22,23] and Ytterbium [24] are also accomplished Bose Einstein condensates.

The development of cold atomic physics include Bose-Einstein condensation gives wide study pool of classical and quantum mechanical physics [3] [25]. In the magneto optical trap, parametric resonance [26], multiple sub-Doppler cooling [27] and variety studies are reported. Furthermore the Bose-Einstein

condensation is a unique sample to study variety quantum mechanical phenomenon. The atoms that have negative scattering length, for example ^{85}Rb, cannot exceed the critical temperature of BEC by the evaporation. However the scattering length can be tuned by magnetic field which is called Feshbach resonance [28] [29], the ^{85}Rb BEC is achieved by the Feshbach resonance [20] and the mixtures with different aomts are also formed molecular cold system [30–32]. The Feshbach resonance is also applied to the Fermion atoms to make molecular BEC [33–35] and it is studied as the BEC-BCS crossover [36]. The cold atomic cloud and the Bose Einstein condensation with optical dipole trap or optical lattices are the amazing tool to study variety physical systems [37, 38]. The lattices with atoms become a simulator of solid system [39, 40], the Bloch oscillator [41], quantum motion [42], low dimensional physics and etc.. The area of cold atomic system is too wide to mention it all and the subject to study with atomic sample is spreading widely now a days.

1.2 Outline

In this thesis, the experimental progress of ultra cold atoms toward Bose-Einstein condensates in magnetic traps lowered temperature by rf evaporative cooling are described. Though the Bose-Einstein condensation could not be obtained, various methods are tried experimentally for that. The experimental precesses and the results of magneto-optical trap, cMOT, molasses cooling, optical pumping, magnetic trap, time-averaged orbiting potential trap, rf-evaporative cooling and optical dipole trap are introduced.

In chapter 2, the theoretical backgrounds for understanding the cold atomic systems are described. The simple overview of Bose Einstein condensation, the force on the atoms in a optical field and magnetic field, the trapping mechanisms of MOT, magnetic trap, and optical dipole trap are included.

The experimental setup is described in chapter 3. All the equipments, assembling the component and working procedure are explained. The experimental system is consisted of many optics, electronics and other experimental equipments, the correct combination of that is very important.

The experimental results are in chapter 4. The process of experiments and the results are described and analyzing the data. And chapter 5 conclude the thesis and the ^{87}Rb line data, mathmetica analysis program and experimental procedures are in appendix.

Chapter 2

Theoretical Overview

2.1 Bose-Einstein Condensation

The Bose-Einstein distribution [43] for non-interacting bosons in thermodynamic equilibrium is given by

$$N_i = \frac{1}{e^{(\epsilon_i - \mu)/kT} - 1}, \tag{2.1}$$

where, ϵ_i is the energy of the single particle state of the potential and μ is the chemical potential [44]. When the temperature is sufficiently low, the number will be quite large. In this case the exponential term $e^{(\epsilon_i - \mu)/kT}$ is very close to 1, which implies that the term of $(\epsilon_i - \mu)/kT$ is very small. Therefore, the exponential term could be expand in a Taylor series and keep only the first two terms,

$$N_i = \frac{1}{1 + e^{(\epsilon_i - \mu)/kT} - 1} = \frac{kT}{\epsilon_0 - \mu}. \tag{2.2}$$

The chemical potential μ must be equal to ϵ_0 at $T = 0$. The general condition to determine the chemical potential μ is the sum of the Bose-Einstein distribution over all states;

$$N = \sum_i \frac{1}{e^{(\epsilon_i - \mu)/kT} - 1}. \tag{2.3}$$

In practical, it's usually easier to convert the sum to an integral;

$$N = \int_0^\infty g(\epsilon) \frac{1}{e^{(\epsilon_i - \mu)/kT} - 1} d\epsilon \tag{2.4}$$

The function $g(\epsilon)$ is the number of single particle states per unit energy in a box of volume V;

$$g(\epsilon) = \frac{2}{\sqrt{\pi}} (\frac{2\pi m}{h^2})^{3/2} V \sqrt{\epsilon}. \tag{2.5}$$

Unfortunately, the integral 2.4 cannot be performed analytically. The easy way is guessing the value of chemical potential. As discussed above, at the low temperature the chemical potential is very small. Suppose the value of chemical potential is zero and change the variables to $x = \epsilon/kT$, that gives

$$N = \frac{2}{\sqrt{\pi}} (\frac{2\pi mkT}{h^2})^{3/2} V \int_0^\infty \frac{\sqrt{x} dx}{e^x - 1}. \tag{2.6}$$

This integral yields the formula

$$N = 2.612(\frac{2\pi mkT}{h^2})^{3/2}V. \tag{2.7}$$

This result is wrong because the number of atoms depends on the temperature at this equation. However the equation is came from the assumption that $\mu = 0$, the equation is correct at only one particular temperature T_c. At temperature higher than the T_c, the chemical potential is negative and all of the atoms are in excited sates. At temperature lower than the T_c, the chemical potential is very close to zero. This formula can be written simply as

$$N_{excited} = (\frac{T}{T_c})^{3/2}N \tag{2.8}$$

And the rest of the atoms must be in the ground state,

$$N_0 = N - N_{excited} = [1 - (\frac{T}{T_c})^{3/2}]N. \tag{2.9}$$

The transition temperature or critical temperature of Bose-Einstein condensation [45] is given by

$$kT_c = 3.3125\frac{\hbar^2 n^{2/3}}{m}, \tag{2.10}$$

where $n = N/V$ is the number density. And the useful concept of defining BEC is the phase space density which is defined as the number of particles contained within a volume equal to the cube of the thermal de Broglie wevelength, $\lambda_{dB}^3 = (2\pi\hbar^2/mkT)^{3/2}$. The phase space density is given

$$\rho = n(\frac{2\pi\hbar^2}{mkT})^{3/2} = n\lambda_{dB}^3. \tag{2.11}$$

For the criterion of Bose-Einstein condensation, the phase space density is over 2.612. The concept of forming Bose-Einstein condensation is well represented at the cartoon of Fig.2.1.

At a high temperature, a weakly interacting gas can be treated as a system of billiard balls. As the temperature lowers, the atoms can be regarded as wavepachets with the de Broglie wave length λ_{dB}. At the BEC transition temperature T_c, the wave length becomes comparable to the distance between the atoms and BEC forms. And below the transition temperature, the thermal cloud fraction disappears leaving a pure Bose-Einstein condensation.

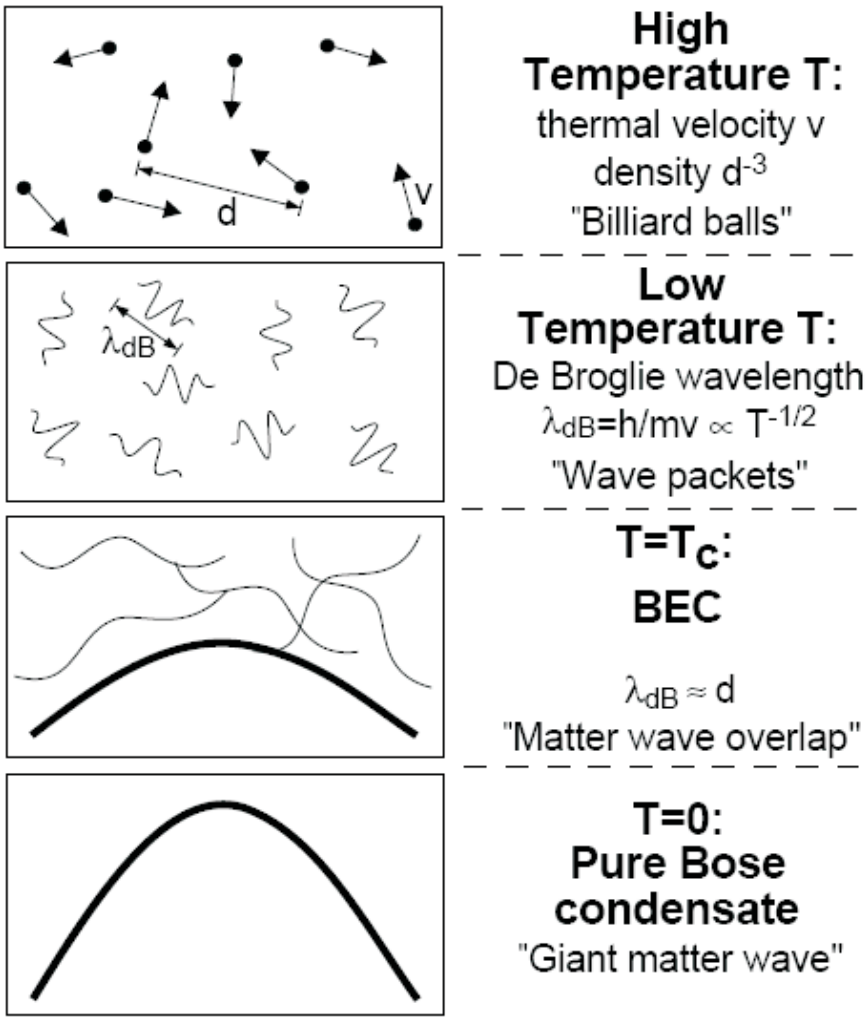

Figure 2.1: A diagram of the criterion of Bose-Einstein condensation. In a high temperature the atoms act like a billiard balls. In a simplified quantum description, the the atoms can be regarded as a wave packets with a de-Broglie wave length $\lambda_D B$ in a low temperatur. At a BEC transition temperatur, $\lambda_D B$ becomes comparable to the atomic distance and a Bose-Einstein condnsate forms [46].

2.2 Magneto Optical trap

2.2.1 Force on Two level Atoms in a laser light field

The force on an atom in a laser light field is defined as the expectation value of the quantum mechanical force operator $\mathtt{F}$ as follows,

$$F =< \mathtt{F} >= \frac{\mathtt{d}}{\mathtt{dt}} < \mathtt{p} > \tag{2.12}$$

.

Generally the quantum version of Newton's laws is embodied in the Ehrenfest theorem [47], a simple statement that the expectation value of an operator must correspond to the behavior of its classical counterpart. The commutator of a Hamiltonian H and a momentum p is $[H, p] = i\hbar\frac{\partial H}{\partial z}$. Where the operator p is replaced by $-i\hbar(\partial/\partial z)$. The force is thus given by

$$F = - < \frac{\partial H}{\partial z} > . \tag{2.13}$$

The Hamiltonian represented by the vector potential is expressed as follows.

$$H(t) = -e\vec{\varepsilon}(\vec{r}, t) \cdot \vec{r}. \tag{2.14}$$

Where $\vec{\varepsilon} = \vec{A}/c$ and $\vec{A}$ is the vector potential. Then the force is

$$< \mathtt{F} >= \mathtt{F} = \mathtt{e} < \frac{\partial}{\partial \mathtt{z}}(\tilde{\varepsilon}(\tilde{\mathtt{r}}, \mathtt{t}) \cdot \tilde{\mathtt{r}}) > . \tag{2.15}$$

The wave-length of the laser field is much larger than the size of the atom, we can neglecting the spatial variation of the electric field over the size of an atom - that is the electric dipole approximation. Then the force is

$$F = e\frac{\partial}{\partial z}(< \vec{\varepsilon}(\vec{r},t)\cdot\vec{r} >). \tag{2.16}$$

For a plane wave traveling in the position z direction, the electric field operator is

$$\vec{\varepsilon}(\vec{r},t) = E_0\hat{\epsilon}cos(kz-\omega_l t), \tag{2.17}$$

where $\hat{\epsilon}$ is the unit polarization vector and E_0 is the amplitude of the light field. The coupling element for this case becomes $H(t) = \hbar\Omega cos(kz-\omega_l t)$, where Ω is the Rabi frequency defined by

$$\Omega \equiv \frac{-eE_0}{\hbar} < e|r|g > \tag{2.18}$$

From equation 2.16 and 2.18, the expectation value is evaluated as follow

$$F = \hbar(\frac{\partial\Omega}{\partial z}\rho^*_{eg} + \frac{\partial\Omega^*}{\partial z}\rho_{eg}). \tag{2.19}$$

Note that the force depends on the state of the atom and on the optical coherence between the ground and excited state, ρ_{eg}. The matrix element that defines Ω in equation2.18 is complex, $\frac{\partial\Omega}{\partial z}$ can be split real and imaginary part so that $\partial\Omega/\partial z = (q_r + iq_i)\Omega$.

Then the expression for the force becomes

$$F = \hbar q_r(\Omega\rho_{eg}^* + \Omega^*\rho_{eg}) + i\hbar q_i(\Omega\rho_{eg}^* - \Omega^*\rho_{eg}). \tag{2.20}$$

The expression of the force in equation 2.20 is the general form that can be used to find the force for any particular situation. The decay (or excite) rate coefficient $\rho_{eg} = \frac{i\Omega}{2(\Gamma/2-i\delta)(1+s)}$ is put into the equation 2.20, a steady state solution is

$$F = \frac{\hbar s}{1+s}(-\delta q_r + \frac{1}{2}\Gamma q_i). \tag{2.21}$$

The saturation parameter s is given by

$$s \equiv \frac{|\Omega|^2}{2|(\Gamma/s - i\delta)|^2} = \frac{s_0}{1+(2\delta/\Gamma)^2}, \tag{2.22}$$

where the on-resonance saturation parameter $s_0 = I/I_s$ and $I_s = \pi hc/3\lambda^3\tau$. The first term in equation 2.21 is proportional to the detuning δ and the second term is proportional to the decay rate Γ. For zero detuning, the force becomes

$$F = \frac{\hbar k\Gamma}{2}\frac{s_0}{s_0+1}. \tag{2.23}$$

It is simply proportional to the momentum per photon $\hbar k$ and the scattering rate Γ. By contrast, for the case of the detunning δ is not zero and atoms are in a standing wave, the equation 2.21 becomes

$$F_{dip} = \frac{2\hbar k\delta s_0 sin2kz}{1+4s_0 cos^2 kz + (2\delta/\Gamma)^2}. \tag{2.24}$$

The equation 2.12 represent the radiation force on the atom and the equation 2.13 is the dipole force when the atom is on the far detunned laser light field.

2.2.2 Magneto Optical Trap

The magneto optical trap(MOT) was first demonstrated in 1987 [48]. The operation of a MOT depends on both inhomogeneous magnetic fields and light field. The Doppler effect, Zeeman shift and the selection rule for optical pumping are also important concepts for trapping neutral atoms. The phase space density of alkali atom vapor compressed up to 15 order of magnitude [49].

Consider the atomic transitions with the simple scheme of $J_g = 0$ to $J_e = 1$, there are three magnetic sub-level in excited state in a linear inhomogeneous magnetic field created by a pair of anti-helmholtz coil. The frequency of light field is red detunned from the atomic resonant frequency because of the Doppler shift. So that the escaped atoms from the trap center are forced by red detunned light. However the velocities of the each atom are not the only value, the detuning of the light field is spacial difference made by linear magnetic field using Zeeman shift [50]. The schematic diagram of the MOT is shown at Fig. 2.2.

The excited state is split into three magnetic sub-levels, $M_e = +1, 0, -1$, by the Zeeman shift. If the polarization of the laser beam is σ^+, for instance, the atomic state have to be excited from the $M_g = 0$ to the $M_e = +1$. An atom located at the $+z$ position is tend to be affected by the σ^- beam, on the other

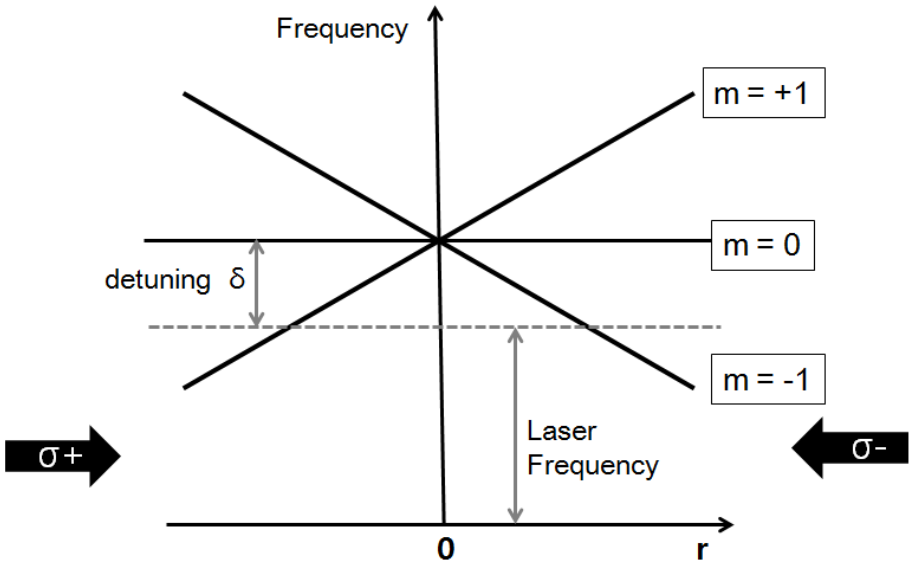

Figure 2.2: The schematic diagram of a magneto optical trap. It is the simple case of the transition between $J_g = 0$ state to $J_e = 1$ state. A red detuned and circular polarized laser is shined to the atoms. Atoms move to the left, it absorb the $\sigma+$ laser comes from left. On the order hands, The atoms at the right are force by the $\sigma-$ laser from the right. The split atomic excited state is due to the magnetic field generated by a pair of anti-Helmholtz coils.

hand, the σ^+ beam forced at $-z$ position for the red detuned light field. The spacial difference of the light force make the atoms cooled and trapped by a MOT.

The total force on the atoms in a MOT is given by $\overrightarrow{F} = \overrightarrow{F}_+ + \overrightarrow{F}_-$, where

$$\overrightarrow{F}_\pm = \pm\frac{\hbar\overrightarrow{k}\gamma}{2}\frac{s_0}{1+s_0+(2\delta_\pm/\gamma)^2} \tag{2.25}$$

and the detuning $\delta_\pm$ for each laser beam is given by

$$\delta_\pm = \delta \mp \overrightarrow{k}\cdot\overrightarrow{v} \pm \mu' B/\hbar \tag{2.26}$$

.

The $\mu' \equiv (g_e M_e - g_g M_g)\mu_B$ is the effective magnetic moment. The Doppler shift $-\overrightarrow{k}\cdot\overrightarrow{v}$ and the Zeeman shift $\mu' B/\hbar$ both have opposite signs for opposite beam.

In a MOT, there is useful definition of special values of temperature associated with laser cooling. The highes of these temperature is related atomic velocity. The Doppler shift puts the atoms at the boundary of the absorption light. The corresponding temperature is

$$k_B T_c = \frac{M\gamma^2}{k^2} \tag{2.27}$$

and is typically several mK.

The next temperature corresponds to the energy associated with the natural line width of the atomic transition. It is given by

$$k_b T_D = \frac{\hbar\gamma}{2}. \tag{2.28}$$

The atoms in a near resonant laser field, photons emit from the atom to random direction. The integration of the energy of photons, the averaged kinetic energy from the emitted photons is related on the natural linewidth and the detuning of laser field. It is a limit of ceratin laser cooling process and often called Doppler limit and the temperature called the Doppler temperature. For the Rb atoms in the $\Gamma/2$ detuned laser field, the Doppler temperature is minimum and 143 μK.

The last characteristic temperature corresponds to the energy of a single photon and named recoil energy. In the absorption process of a single photon, the atoms obtain a recoil momentum of $\hbar k$. The recoil temperature is given by

$$k_B T_r = \frac{\hbar^2 k^2}{M} \tag{2.29}$$

and is generally regarded as the lower limit of laser cooling process. For the Rubidium atoms with the $780nm$ transition line, the recoil limit is $370nK$. The density [51] and temperature are limited in optical process to lower up to critical temperature of BEC.

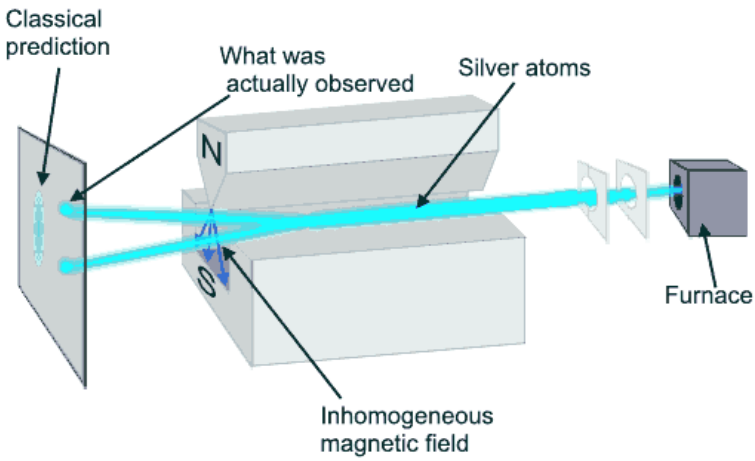

Figure 2.3: A schematic diagram of the Stern-Gerlach experiment. It is the first demonstration of the interaction between atomic multipole moment and inhomogeneous magnetic field with silver atomic beam.

2.3 Magnetic Trap

As discussed above, the MOT process have a limitation to lower the temperature of trapped atoms. It is needed to investigate new type of trapping and cooling methods to overcome the limitation of the MOT procedure. The most widely used trapping methods to have a possibility lowering the temperature below recoil limit are the pure magnetic trap, the optical dipole trap and the hybrid trap that employs the magnetic trapping and optical dipole potential both. In this section, the magnetic trapping is discussed and the optical dipole potential will be mentioned the next section.

The Stern-Gerlach experiment in 1924 first demonstrate the mechanical action of a particle having magnetic moments in the inhomogeneous magnetic field [52]. An atom with a magnetic moment $\vec{\mu}$ is forced by magnetic field as

follow,

$$\vec{F} = \bigtriangledown(\vec{\mu} \cdot \vec{B}). \tag{2.30}$$

The magnetic confinement of neutral atoms depends on the interaction between an inhomogeneous magnetic field and an atomic multipole moment. The magnetic trapping of neutral atoms was first demonstrated in 1985. The potential of magnetic field with atomic magnetic dipole moment is given by

$$H = -\mu B = m_F g_F \mu_B |B| \tag{2.31}$$

From the Maxwell's equation, the magnetic local maxima dose not exist and trapping atoms by the local maxima is forbidden [53]. The only possibility of trapping neutral atoms magnetically occurs at magnetic local minimum. However, at the point of zero value of magnetic field the spin flip is occurred known as Majorana spin flip [54]. Magnetic trapping potentials for ultra cold atomic cloud include achieving Bose-Einstein condensation must have solutions to prevent atomic loss due to the spin flip.

2.3.1 Magnetic Spherical Quadrupole Trap

The most simple way to produce magnetic potential is a magneitc spherical quadrupole field created by an anti-Helmholtz(AH) coil pair [55]. The magnitude of the magnetic spherical quadrupole field is given by

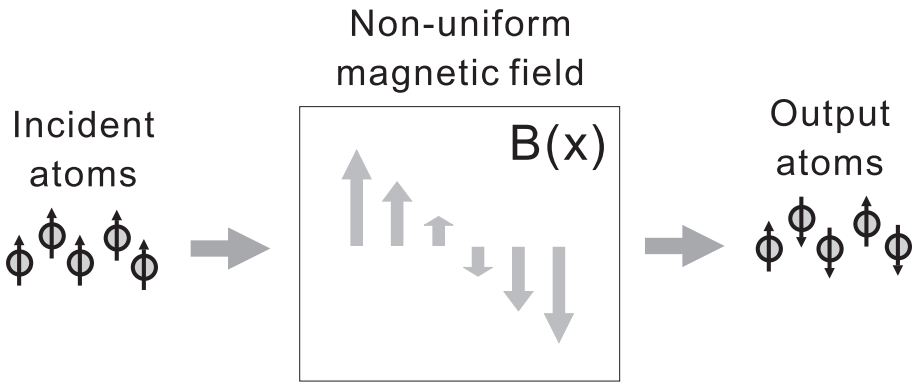

Figure 2.4: The spin-flip transition is occurred when atoms moving in a non-uniform magnetic field [58].

$$B = A\sqrt{\rho^2 + 4z^2}, \tag{2.32}$$

where $\rho^2 = x^2 + y^2$ and the field gradient A is a constant. The magnitude of the magnetic field at the center is zero and increased linearly along any axis, so that the spherical quadrupole trap is also called linear trap. When the coils are separated by 1.25 times their radius, such a trap has equal depth in the radial and longitudinal directions [56].

The magnetic spherical quadrupole coil has many advantages that are easily creating, large potential area and good evaporative efficiency. And the AH coil pair of magnetic spherical quadrupole trap could be shared with the MOT coil, it is very convenient to transfer the atoms from a MOT to magnetic trap. However the magnetic spherical quadrupole trap has a critical problem which is the escaping of atoms near the center of the trap by the majorana spin flip [57].

In 1932 E. Majorana develops an elegant formalism for the solution of the time dependent Schrödinger equation of an object with angular momentum number J and magnetic moment m in a varying external magnetic field B. In the spin flip transition, two characteristic frequencies have important role. The first is Larmor frequency of the atomic dipole moment $w_L = gmB/\hbar$ and the second one is the rotating frequency of the magnetic field in the rest frame of the atom w_B. The atom or an object with angular momentum J change its magnetic sub-state, i.e. a spin flip, following the magnetic quantum axis. The spin flip probability P depends on the ratio $k = w_L/w_B$ and the probability is given by

$$P = exp(-k\pi/2). \tag{2.33}$$

In a magnetic quadrupole trap, a zero magnetic field is exist at the center. The atom lose its spin axis passing through near the trap center and escape from the magnetic quadrupole potential by the spin flip.

2.3.2 Time Averaged Orbiting Potential(TOP) Trap

Variety ideas are suggested and applied to achieve Bose-Einstein condensation or ultra cold atoms for trapping without majorana spin flip problem. Schematic diagram of several traps are shown at Fig.2.6.

We used the time averaged orbiting potential(TOP) trap configuration. It is easy to establish and very convenient to loading atoms from a MOT or a

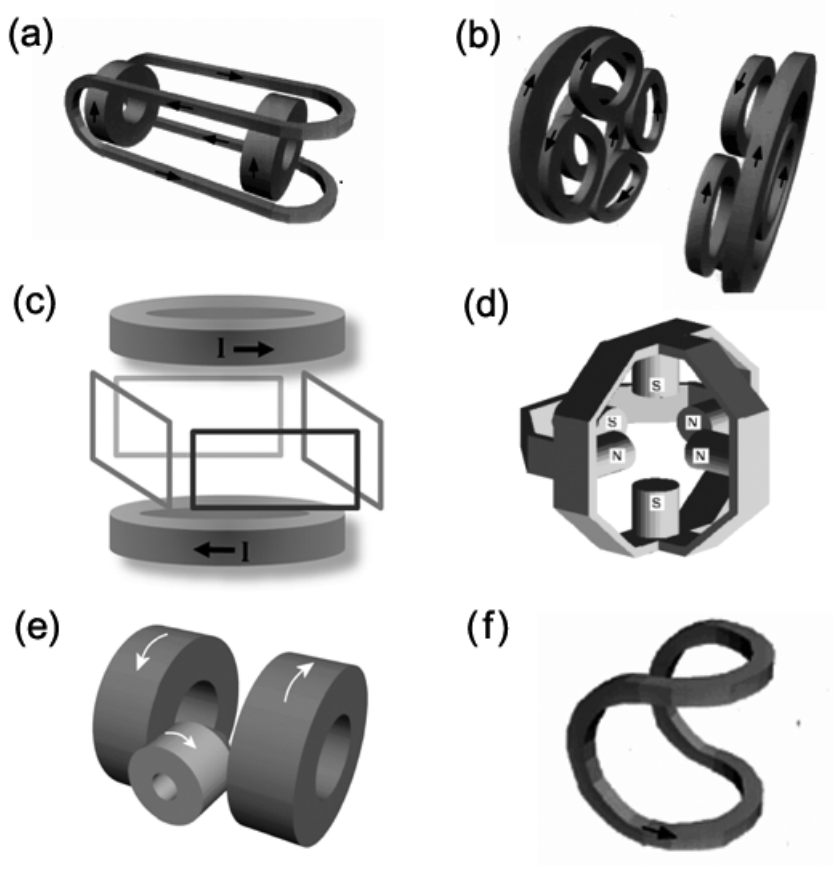

Figure 2.5: Schematic diagrams of variety magnetic traps. (a) Ioffe Pritchard trap [16] (b) Clover-leaf trap [59] (c) Time-averaged orbiting potential(TOP) trap [60] (d) Permanent magnetic trap [61] (e) Quadrupole Ioffe configuration(QUIC) trap [62, 63] (f) Base ball trap [64, 65]

magnetic spherical quadrupole trap. In this section, we investigate the TOP trap theoretically.

In 1995, ^{87}Rb atoms are first trapped by TOP trap [60] and Bose-Einstein condensates are achieved [15]. The TOP trap is consist of the anti-Helmholtz coil pair and the rotating and spatially uniform bias field. The rotating bias field keep the atomic spin in a non-zero magnetic field before it escaped by spin flip. The frequency of the rotating field is chosen to be much greater than that of atomic motions and less than that of transitions between magnetic sub-states. Typically the frequency of atomic motion is order of 10^2 Hz and the frequency of the atomic sub-state is order of 10^6 Hz or more, and the frequency of the bias field is in the kilohertz range.

The TOP trap is described as the combination of a quadrupole field and a rotating bias field as follow,

$$\mathbf{B} = (B^{'}x + B_0 cos\omega t, B^{'}y + B_0 sin\omega t, -2B^{'}z). \tag{2.34}$$

To determine the effective potential, the strength of the magnetic field is evaluated as follow,

$$B(t) = [(B^{'}x + B_0 cos\omega t)^2 + (B^{'}y + B_0 sin\omega t)^2 + (2B^{'}z)^2]^{1/2} \tag{2.35}$$

$$\simeq B_0 + B^{'}(xcos\omega t + ysin\omega t) + \frac{B^{'2}}{2B_0}[x^2 + y^2 + 4z^2 - (xcos\omega t + ysin\omega t)^2]. \tag{2.36}$$

The time average of the magnitude of the TOP field over a rotation period is given by

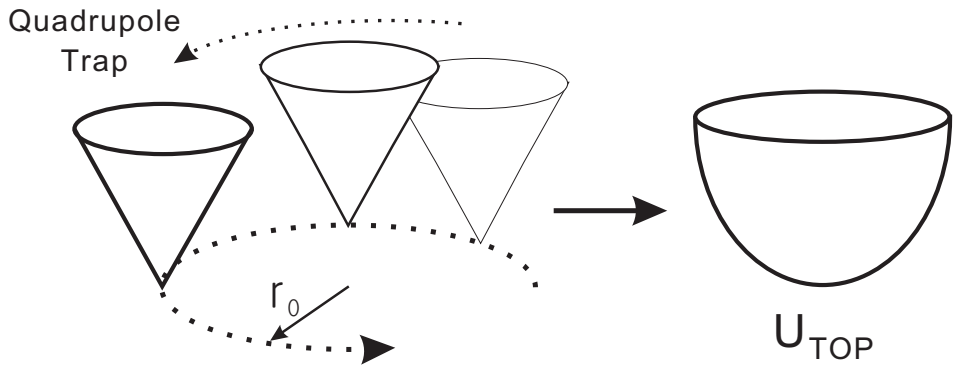

Figure 2.6: Schematic diagram of the principle of TOP trap. The bias field make the quadrupole field rotate with the to form a harmonic potential. There are no zero point in the TOP trap

$$< B >_t = \frac{\omega}{2\pi} \int_0^{2\pi/\omega} dt B(t) \simeq B_0 + \frac{B'^2}{4B_0}(x^2 + y^2 + 8z^2). \qquad (2.37)$$

The important feature of this result is that the TOP filed never vanishes and there is no longer a zero point in the trap.

2.4 Evaporative Cooling

The temperature reached by laser cooling are impressively low, but it has the limitations called Doppler limit or recoil limit that is not enough to produce Bose-Einstein condensation. There are no cooling mechanism in the magnetic trap, a new method is needed. In the experiment, the temperature of trapped atoms is lowered by evaporative cooling. The basic physical effect in evaporation is that, if particles escape with an higher energy than the average energy of the system, the remaining particles are cooled [66, 67].

The evaporative cooling mechanisms are introduced here below.

1. Direct contact with walls

The simplest scheme for evaporation is to close a sticky walls to the atomic cloud to absorb the high energy tail of the distribution. This method was used in the first realization of electromagnetic confinement of neutral particles [68] and in the hydrogen experiment [69].

2. Lowering the Total Trapping Potential

The high energy atoms escape the trap when the trapping potential is lowered. This have been commonly used in the optical dipole trap and it was first demonstrated in Stanford group [70]. But this method has a disadvantage that the collision rate become very small during the decompression caused of the decreased density. One might have to repeat several compression and evaporation cycles.

3. Saddle Point of the Potential

The disadvantage of the lowering trapping potential is due to the proportionality between the trap depth and confinement. This was avoided by lowering only the axial trapping potential and it was first used in the hydrogen experiments [71]. The saddle point method is a 1D selective cooling because it selects the atoms due to their axial energy.

4. Radiative Evaporation

The experiment of rf spectroscopy to determine the energy distribution of magnetically trapped atoms was demonstrated in 1988 [72]. And they suggested that this method could be used to perform evaporative cooling [73] and mentioned three advantages compared with the saddle-point mothod : (1) The trap potential does not modified during the evaporation. (2) The escape rate and the potential are easily controlled. (3) The evaporation area is given by a shell of potential, thus it is not limited to the saddle point. The radiative evaporation method is widely used in the magnetically trapped atomic experiment. The schematic illustration of rf-evaporation is shown at Fig.2.4. In the experiment the frequency and evaporation time are selected for optimized pass to form a Bose Einstein condensate [74].

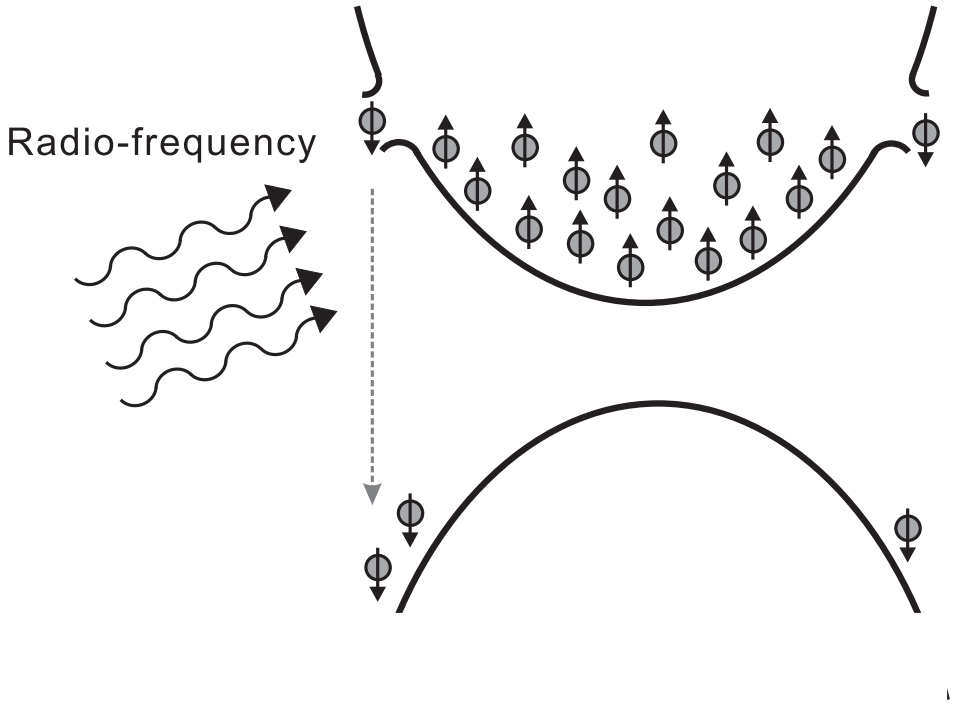

Figure 2.7: An illustration of rf-evaporative cooling. The magnetic moment of atoms in the low field seeking state is transferred to the high field seeking state by a resonant radio frequency field. The hot atoms escape from the trap with energy over the average energy of system. The total energy of remained atoms in the trap is lowered than the energy before evaporation.

2.5 Dipole Trap

2.5.1 Gaussian Beam

An expression for the complex amplitude $U(r)$ of the Gaussian beam is obtained by the equation 2.38 [75].

$$U(r) = A_0 \frac{W_0}{W(z)} exp[-\frac{\rho^2}{W^2(z)}] exp[-ikz - ik\frac{\rho^2}{2R(z)} + i\zeta(z)] \tag{2.38}$$

Where, W_0 is the beam waist, $W(z)$ is the beam width at the position z, ρ is the radial distance and $R(z)$ is the wavefront radius of curvature. And the beam parameters are able to calculated as follow,

$$W(z) = W_0[1 + (\frac{z}{z_0})^2]^{1/2} \tag{2.39}$$

$$R(z) = z[1 + (\frac{z_0}{z})^2] \tag{2.40}$$

$$\zeta(z) = tan^{-1}(\frac{z}{z_0}) \tag{2.41}$$

$$W_0 = (\frac{\lambda z_0}{\pi})^{1/2} \tag{2.42}$$

.

z_0 is the Rayleigh range and λ is the wavelength of the beam. All other parameters are related z_0 and the wavelength. Far from the beam center, when

$z \gg Z_0$, the beam radius increases approximately linearly with z, defining a cone with half-angle θ_0. The beam divergence is defined by the angle $\theta_0 = \frac{2}{\pi}\frac{\lambda}{2W_0}$. The beam has its minimum width at z=0 and the beam radius is grows out of focus. At $z = z_0$ the Rayleigh length, the beam radius is $\sqrt{2}W_0$ that is known as the depth of focus or confocal parameter.

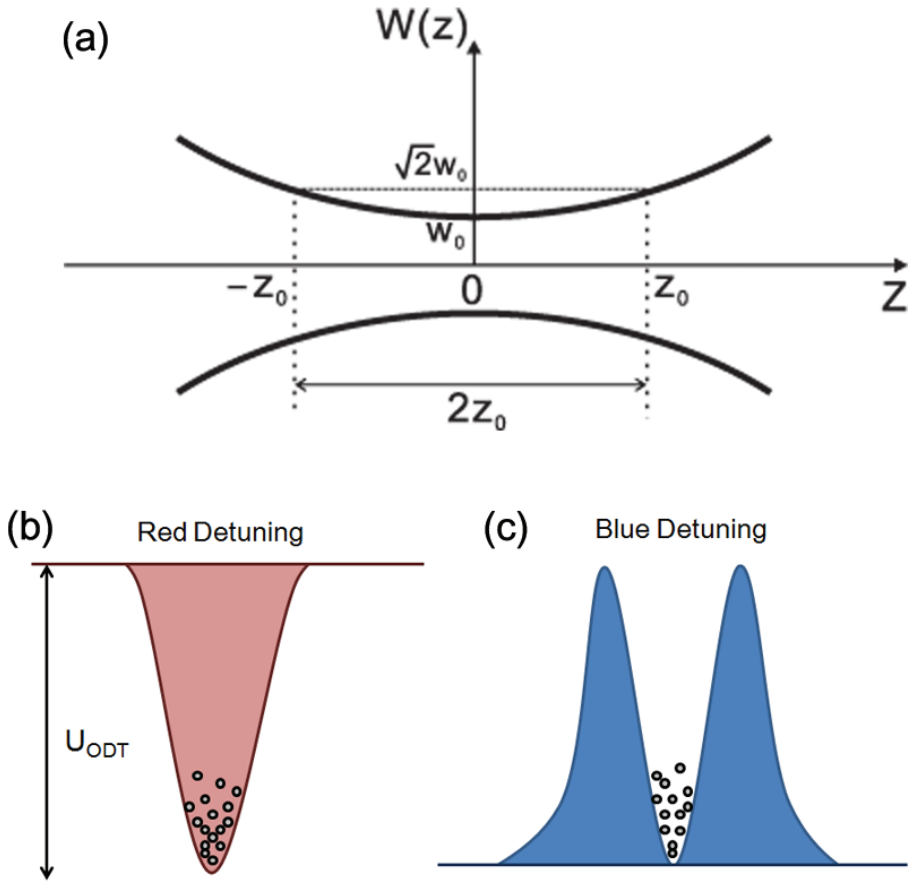

Figure 2.8: (a) The geometry of a gaussian beam. w_0 is the beam waist and z_0 is the Rayleigh range. (b) The optical dipole potential when the frequency of laser is red detuned comparing with the atomic resonance [76, 77]. (c) Optical potential made by blue detuned laser [78, 79].

2.5.2 Optical Dipole Potential

When an atom is placed into laser light, the electric field E induces an atomic dipole moment P. In the usual complex notation $E(r,t) = \hat{e}\tilde{E}(r)exp(-iwt) + c.c.$ and $p(r,t) = \hat{e}\tilde{p}(r)exp(-iwt) + c.c.$ [77, 80]. The amplitude $\tilde{p}$ of the dipole moment is simply related to the field amplitude $\tilde{E}$ by

$$\tilde{p} = \alpha\tilde{E}. \tag{2.43}$$

Here α is the complex polarizability given by

$$\alpha = \frac{e^2}{m_e}\frac{1}{\omega_0^2 - \omega^2 - i\omega\Gamma_\omega} \tag{2.44}$$

where,

$$\gamma_\omega = \frac{e^2\omega^2}{6\pi\epsilon_0 m_e c^3}. \tag{2.45}$$

The interaction potential of the induced dipole moment p in the driving field E is given by

$$U_{dip} = -\frac{1}{2} < pE >= -\frac{1}{2\epsilon_0 c}Re(\alpha)I. \tag{2.46}$$

With the above expression for the polarizability of the atomic oscillator the following explicit expressions are derived for the dipole potential and the scattering rate in the relevant case of large detunings and negligible saturation,

$$U_{dip}(r) = -\frac{3\pi c^2}{2\omega_0^3}(\frac{\Gamma}{\omega_0 - \omega} + \frac{\Gamma}{\omega_0 + \omega})I(r). \tag{2.47}$$

And for the case of multilevel alkali atoms, the optical dipole potential is given by

$$U_{dip}(r) = \frac{\pi c^2 \Gamma}{2\omega_0^3}\left(\frac{2 + A_{pol} g_F m_F}{\Delta_{2,F}} + \frac{1 - A_{pol} g_F m_F}{\Delta_{1,F}}\right) \tag{2.48}$$

where, A_{pol} is the laser polarization($A_{pol} = 0, \pm 1$ for linearly and circularly $\sigma^{\pm}$ polarized light) and the detuning $\Delta_{2,F}$ and $\Delta_{1,F}$ refer to the energy splitting between the particular ground state and the two excited sates, respectively.

The direction of light filed is decided by the dituning. An atom in the red detuned light field is force to the intense region, whereas repelled in the blue detuned light field(Fig. 2.5.1(b),(c)) [81].

Chapter 3

Experimental Setup

3.1 Overview

The experimental setup is designed for realization of ^{87}Rb Bose-Einstein condensation. There are two isotopes of Rubidium in nature that are ^{85}Rb and ^{87}Rb. The ^{85}Rb is 72.2 % and the ^{87}Rb is 27.8 % [82]. The alkali atoms have one electron in the ground state, it is very easy to consider the excited state. Rubidium atom have two main transition line(from s state to p state) named $D1$ and $D2$ line. The frequency of 780 nm $D2$ transition line($5^2S_{1/2} \rightarrow 5^2P_{1/2}$) is used in the experiment because the 780 nm commercial laser diode can be bought easily.

The experimental setup could be divided into four part which are chamber-vacuum part, optics part, magnetic part and computer control part [83] [84].

The experimental chamber is double MOT system and the pressure of

the chamber is below $1 \times 10^{-11} Torr$. The trapped atoms in the 1st chamber is transferred by on resonant pushing laser to the 2nd chamber.

The frequency of lasers are locked to Rb^{87} D2 line that is obtained by saturation absorption spectroscopy(SAS). The frequency and the intensity of the lasers are controlled by acoustic optical modulator(AOM) and turned on and off by mechanical shutters.

The current of anti-helmholtz coils for MOT and magnetic trapping at the 2nd chamber is supplied by 15kW high power DC-supply. Shimming coils are attached for compensating geomagnetic field and undesired external magnetic field.

The AOMs, mechanical shutters, magnetic field and other experimental components are controlled by computer. The control signal is generated by field programable gate array(FPGA).

3.2 Chamber Design and Vacuum

We assembled stainless chamber and glass chamber by 45 cm long narrow pipe that is known as the Double MOT system [85]. A double-MOT system with differential pumping is used to overcome a contradiction about the vacuum. There are several type of chamber design generally used to making ultra cold atomic sample include Bose-Einstein condensation, that are Zeeman slower method, pyramidal trap [86] and the double-MOT system which we employed.

For large number of atoms to trap, sufficient atomic gas in the background is needed. However, for keeping the atomic cloud cold in a trap, it is necessary to scatter as little as possible with other thermal gas in the vacuum, meaning that a low vacuum pressure is important. For this reason, we utilize two chambers connected by a pipe 1cm in diameter and 40 cm long. A 20 l/s ion pump is attached at the first stainless chamber and a 50 l/s ion pump is attached at the 2nd glass chamber. The schemetic diagram of vacuum chambers and lasers is show at Fig.3.2.

For ultra high vacuum(UHV), we spend 1 month to bake out the hole chamber. The 2nd glass chamber is made of pyrex and it is attached cooper vacuum flange by kovar to match thermal expansion between glass and metal. However, the conduction difference between glass and cooper, temperature increase rate is very important when we baked it out. We increase the temperature of 10 °C per 2 hour. We have tried to increase the baking temperature of 10 °C per 2 hour but it broke the glass cell. After 2 weeks baking up to the tem-

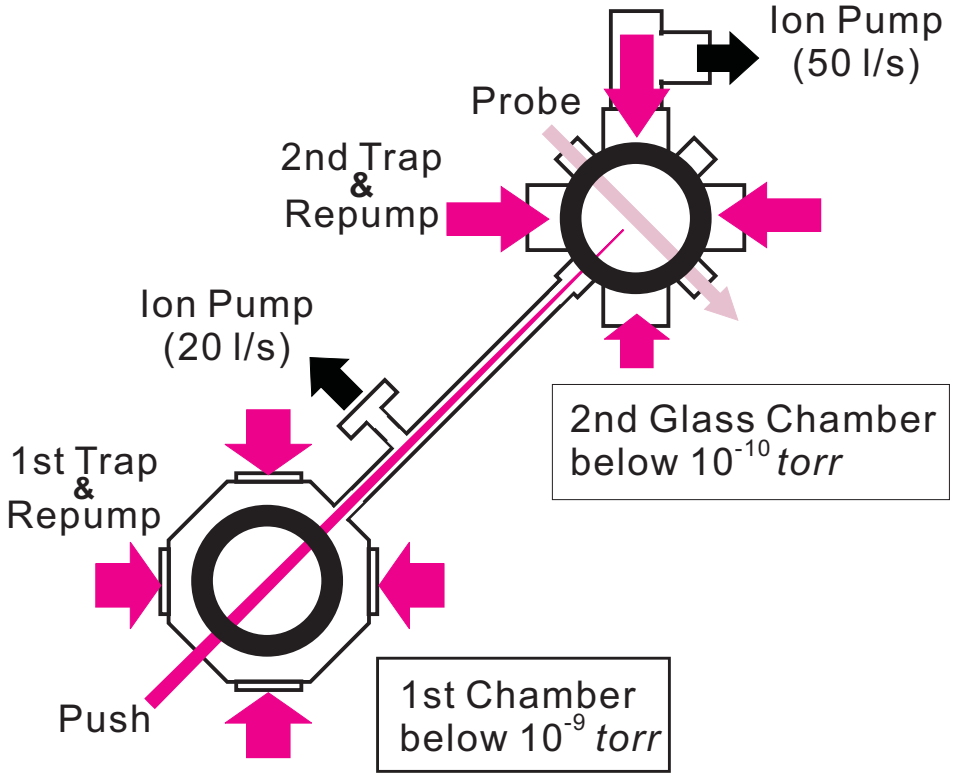

Figure 3.1: A schematic diagram of the vacuum chamber of a double MOT system and laser aligns. The pressure of the 1st chamber is below 10^{-9} *torr* and it of the 2nd glass chamber is below 10^{-10} *torr*.

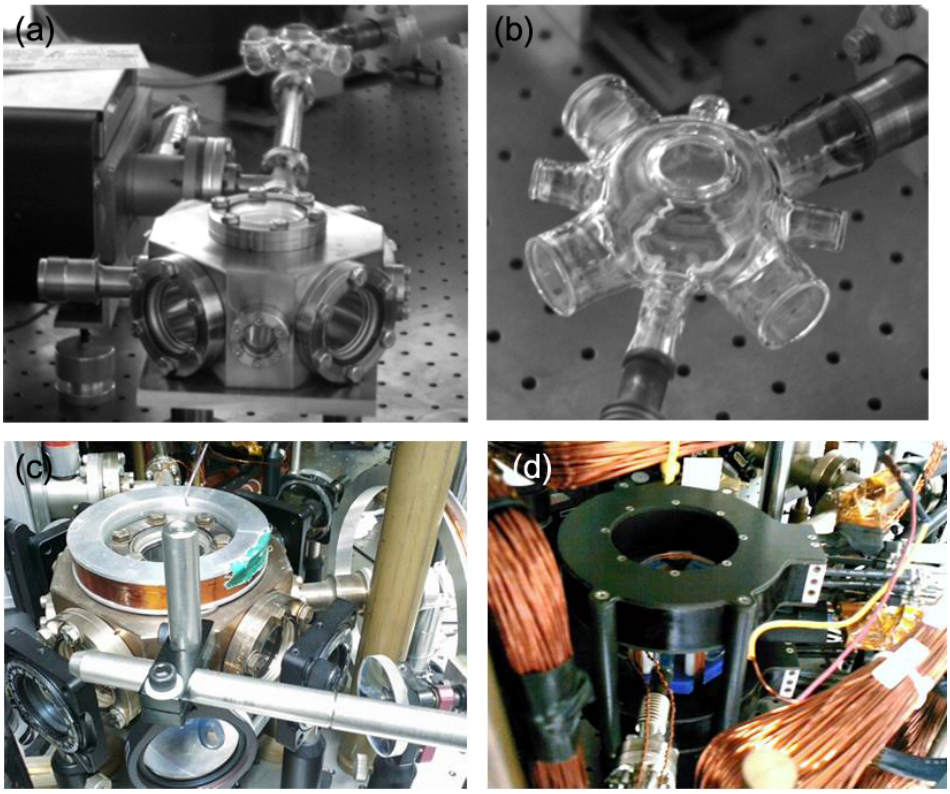

Figure 3.2: photos of (a)the first vacuum chamber and (b)the second vacuum chamber. (c),(d) after assembling all the optics, shimming coils and anti-Helmholtz magnetic coils.

perature of 350 °C and the de-gasing process, the pressure of the 1st chamber reached below 1×10^{-9} torr and that of the 2nd chamber is measured below 1×10^{-11} torr, both values are measurement limit of the ion pump gauge.

3.3 Lasers and Optics

We used lasers for variety purpose which are trapping, repumping, optical pumping, molasses cooling, pushing and probing. The frequency of laser is locked using external cavity with ^{87}Rb D2 line obtained from saturation absorption spectroscopy(SAS). And the detunning is controlled by acoustic optical modulator(AOM).

Three different laser frequencies of the ^{87}Rb D2 line are used in the experiment. There are two ground states(F=1, 2) and four excite states(F=0, 1, 2, 3) in D2 line. The three frequencies are named trap line, repump line and depump line. The trap line is resonant on the transition frequency from the F=2 ground state to the F′=3 state. The trap line laser is used for trapping, pushing and probing atoms. Lasers for trapping at the first and the second chamber are 2Γ red detuned from the trap line frequency. The pushing laser is 1Γ red detuned and the probe laser is on resonance from the trap line frequency. The repump line frequency is resonant on the F=1 ground state to the F′=2 state and the depump line is resonant on the F=2 ground state to the F′=2 state. The ^{87}Rb D2 line and the laser frequencies are shown at Fig.3.3.

All the frequency of the lasers are stabilized by a Littrow type external cavity diode laser(ECDL) system(Fig.3.3). The laser diode and a grating at the ECDL system form a cavity whose length is controlled by a PZT. The frequency reference is obtained by the saturation absorption spectroscopy(SAS, Fig.3.3). The alignment of the SAS and the obtained atomic transition lines are shown

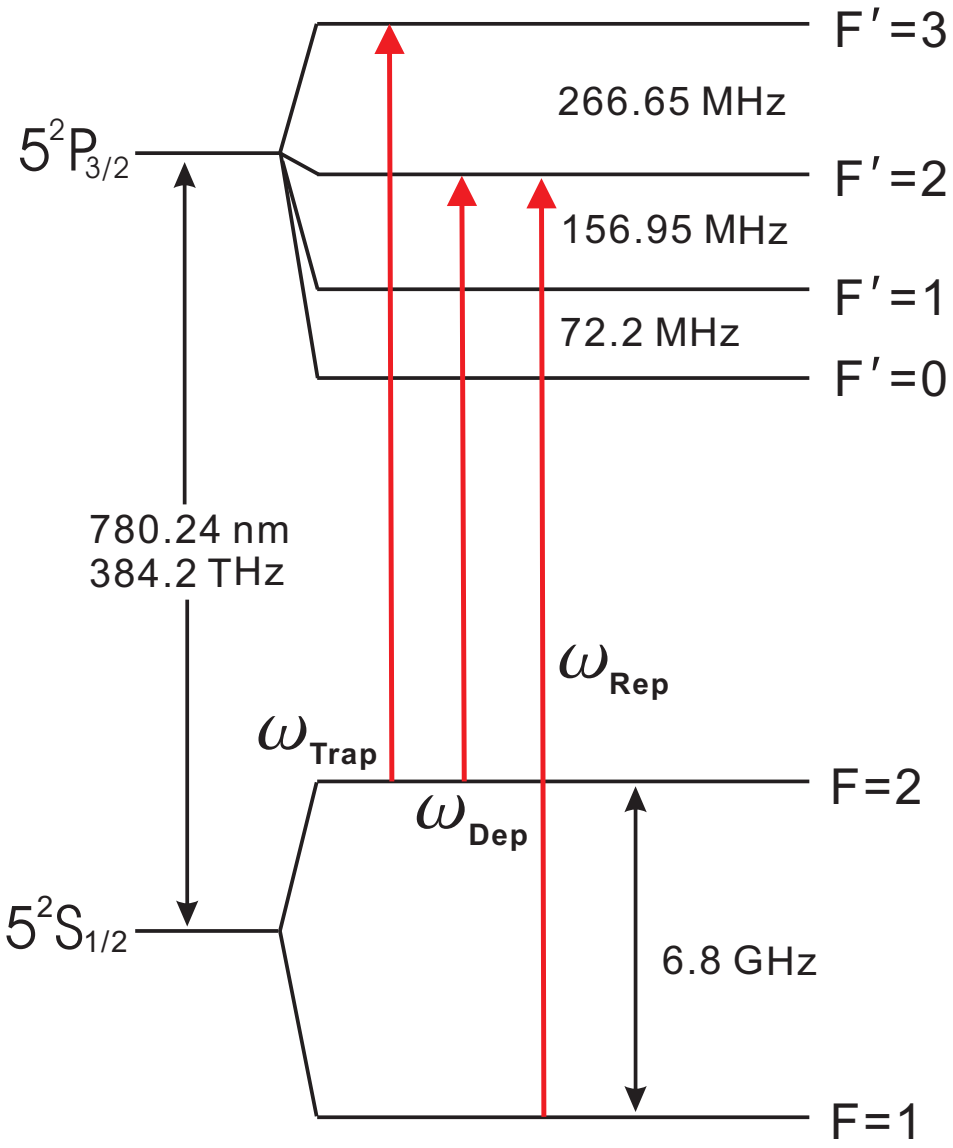

Figure 3.3: The ^{87}Rb D2 line($5^2S_{1/2} \rightarrow 5^2P_{3/2}$) and the laser frequencies in use.

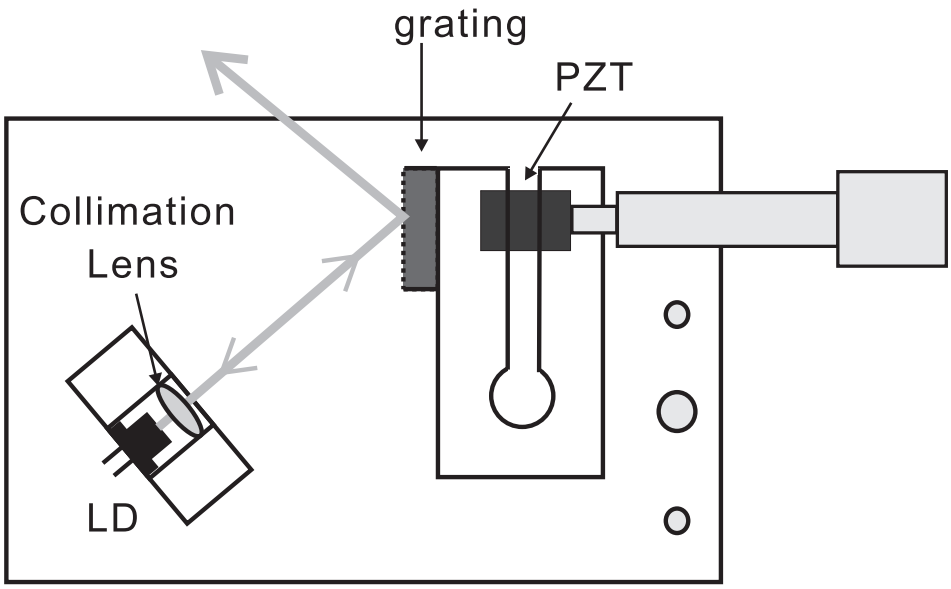

Figure 3.4: A diagram of a External Cavity Diode Laser(ECDL). The laser diode and a grating form a external cavity and the frequency is tuned by controlling the PZT length or LD current.

at fig.3.3. The frequencies are locked within a few megahertz range to the peak of the SAS signal by a lock-in regulator [87].

In practically, five lasers are classified for its purpose that are named 'trap laser', 'repump laser', 'push laser', 'depump laser' and 'probe laser'. In the fist chamber, a trap, a repump and a push laser are used and a trap, a repump, a depump and a probe lasers are worked in the second chamber. A 1W ECDL laser and a tapered amplifier laser system(Toptical, DLX110) generate the trap laser of 2nd trap, the seeding of the 1st trap laser, the depump, the push and the probe laser.

The frequency of the trap laser is red detunned from the 'trap line' of the 87 Rubidium D2 line. The seeding of the trap laser of 1st chamber is amplified

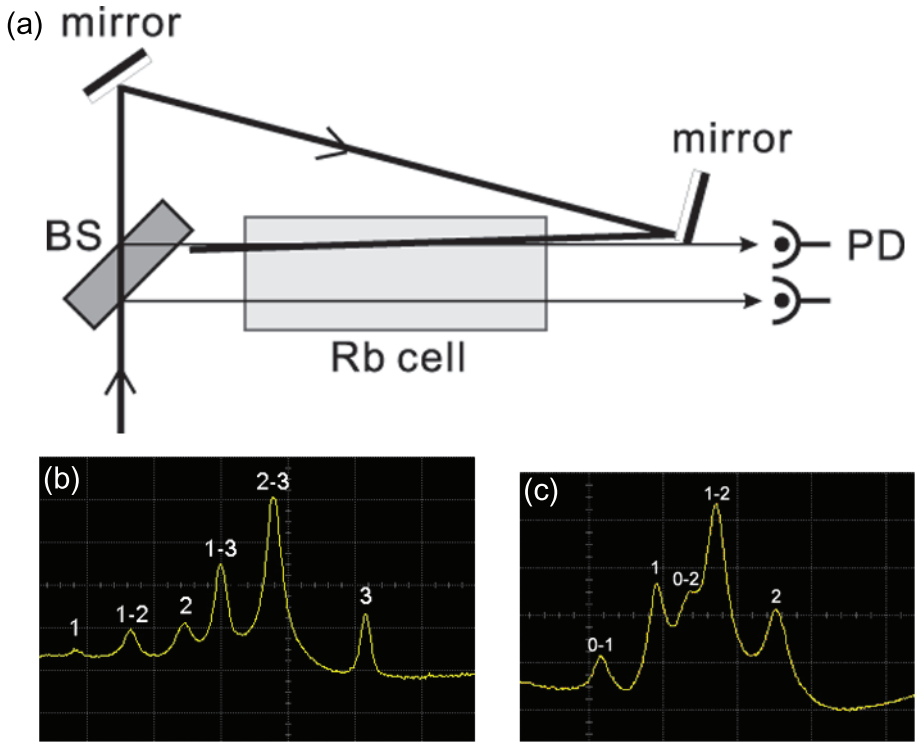

Figure 3.5: A diagram of the saturation absorption spectroscopy(SAS) align. The $S1$ signal could not be absorbed due to the strong pumping laser(S_p) by Rb atoms when the laser frequency is resonant on the atomic transition frequency. The $S2$ signal is the Doppler signal that is used for obtaining a Doppler-free SAS signals. The obtained absorption signal of the transition $F = 2$ to $F^{'}$(b) and the transition $F = 1$ to $F^{'}$ (c).

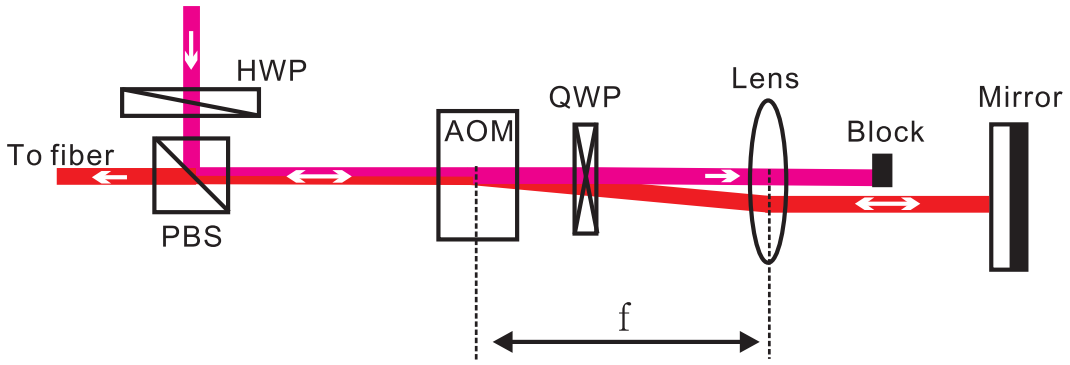

Figure 3.6: The Double pass align of a AOM System. A lens is located at the distance of focal length from the AOM. The laser passing through the AOM and lens return back its coming pass.

by the MOPA(master oscillator power amplifier) laser(SDL, TA30). The total power of the trap laser at the first chamber is about 60mW and the 2nd trap laser is about 50mW. Especially the 2nd trap laser is fiber coupled for formming a gaussian profile which is critical point at the stage of the magnetic loading and the molasses cooling.

The trap laser is needed to change the detuning with controlling the intensity, we use double pass AOM technique [88]. Varying the detunning by a AOM changes the diffraction angle of the out going laser from it, the efficiency of the fiber coupling also is changed. An lens is located after AOM and a mirror is at the distance of the focal length of the lens. The schematic diagram of the double pass aom system is shown at Fig.3.6, it make the detunning and the intensity be controlled independently. The laser beam passing through the AOM at one time is used for depump laser.

The repump laser is resonant on the atomic transition from the $F = 1$

Mater	Slave	Name	Power	detunning	set line
DLX110	MOPA	1st Trap	60 mW	-2.5 Γ	trap line
DLX110		2nd Trap	50 mW	-2.5 Γ	trap line
DLX110		push	5 mW	-2 Γ	trap line
DLX110		probe	1 mW	on resonant	trap line
DLX110		depump	1 mW	on resonant	depump line
DL100	Sanyo LD	repump	30 mW	on resonant	repump line

Table 3.1: The specification of the lasers in use.

state to the $F = 2$ state that is the 'repump line'. We use master-slave system for the repump laser, the master laser is a DL100 type hand-made laser and a 70mW Sanyo laser diode is used as a slave laser.

The push laser passes through the center of the trapped atoms in the 1st chamber. It focused a few cm front and a few mm above the center of the 2nd chamber. The frequency is red detunned 2Γ from the resonance of the trap line for the moving atoms to the 2nd chamber not being forced by the laser.

Two optical table are used in this experiment, one is for $1W$ DLX110 laser and the another is for experimental chambers and other laser and optics. The optical table diagram is shown at fig. 3.3 and fig.3.3.

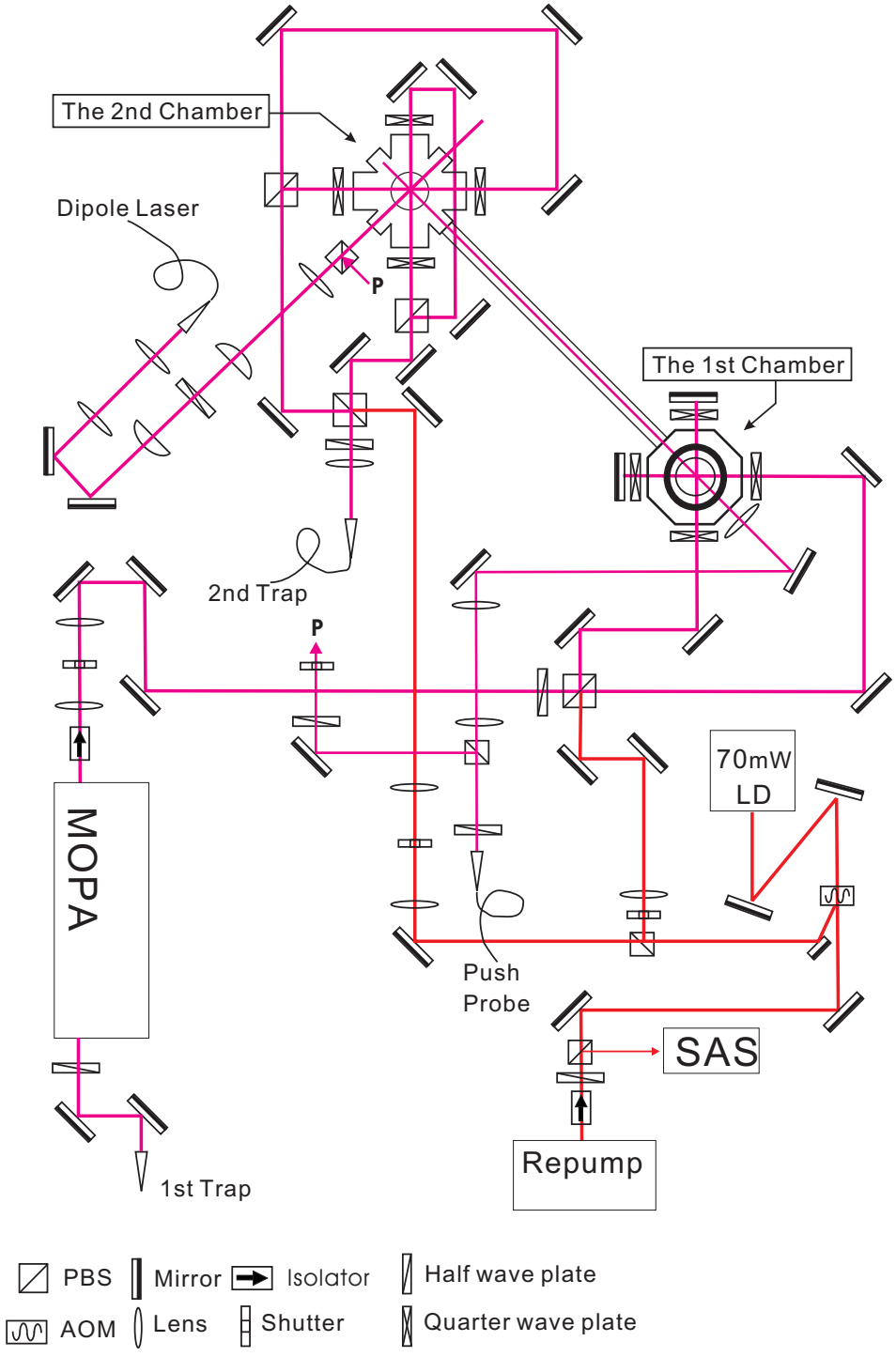

Figure 3.7: A schematic diagram of the experimental optical table

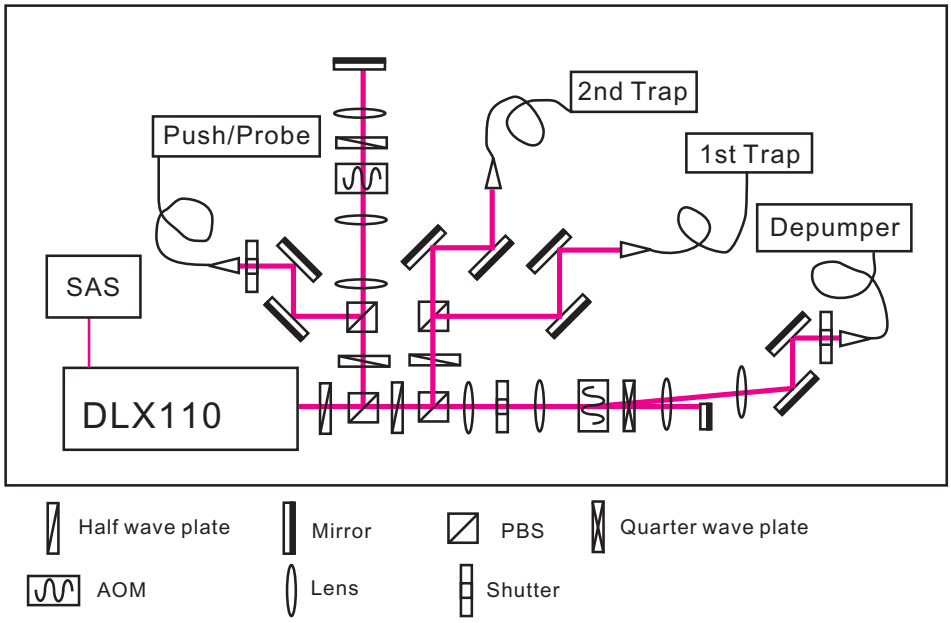

Figure 3.8: A schematic diagram of the laser optical table

3.4 Magnetic Field

The magnetic field gradient of the magnetic spherical quadrupole potential is created by the anti-Helmholtz coil pair that is the same one used for magneto optical trap in the 2nd chamber. The AH coil pair is consisted of a piece of hollow 4mm×4mm square cooper wire and it is water cooled. The coils have 30 turns(6 turns and 5 layers) for each.

A 15kW DC power supply(Lambda EMI) generate the current of the coil. The maximum magnetic field gradient is 270 G/cm at 400 A in the z direction(135G/cm in the radial direction).

An IGBT(insulated gate bipolar transistor) and passive electronic components are assembled as a switch of the power supply. The schematic diagram

of the switch circuit is shown at Fig.3.9. Three power resistors(1Ω,100W) are connected in parallel at the switching circuit for consuming the remaining current in the coil when it is switched off. By the power resistors, the magnetic field is turned off within a few tens of μs. To protect the IGBT switch from high-power electronic shocks, a varistor(TNR 20E391K) is used.

The magnetic field was measured by a gauss meter(Model 5080, F. W. Bell) or a pick-up coil. However the time resolution of the gauss meter is 1 ms which is not enough to measure the turning on and off time, thus the gauss meter is used for measure the strength of the field. The turning on and off time of magnetic quadrupole field are measured by a pick-up coil. The current of power supply(or magnetic field) rise up within a few ms and the IGBT switch turn off the magnetic field less than 10 μs(Fig.3.9 (b)). The turn off time is important for the accuracy of time of flight(TOF) procedure. The resistance of the switch circuit(Fig.3.9 (a)) has important role to reduce the turn off time, that was a few hundred μs before attaching the resistance.

The magnetic field gradient per supplied current is 0.65 G/cm/A that is measured by the gauss meter and also calculated. The calculated geometry of magnetic field created by the AH coil is shown at Fig.3.10.

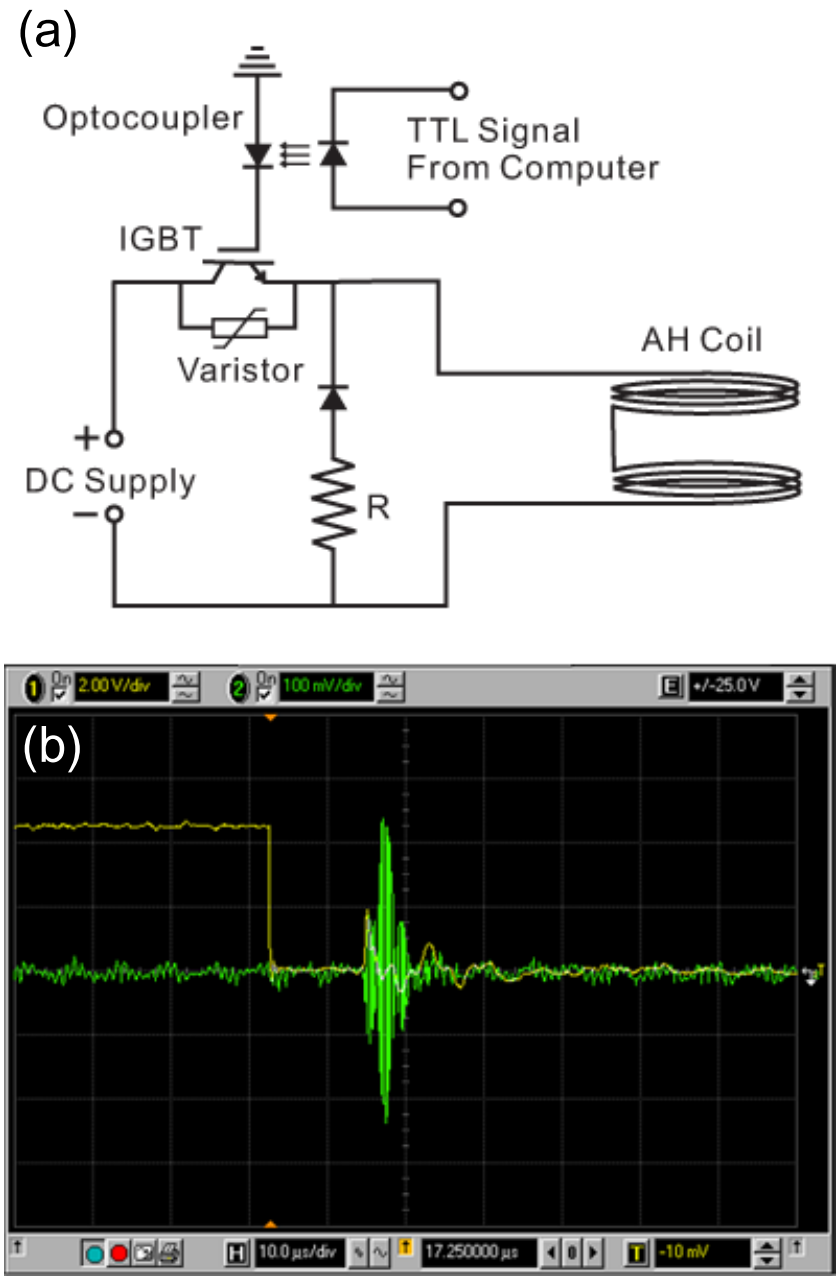

Figure 3.9: (a) The switch circuit of the AH coil pair at the 2nd chamber. R is the three 1Ω, 100W resistances in parallel.(b) The measured magnetic field gradient when it switched off.

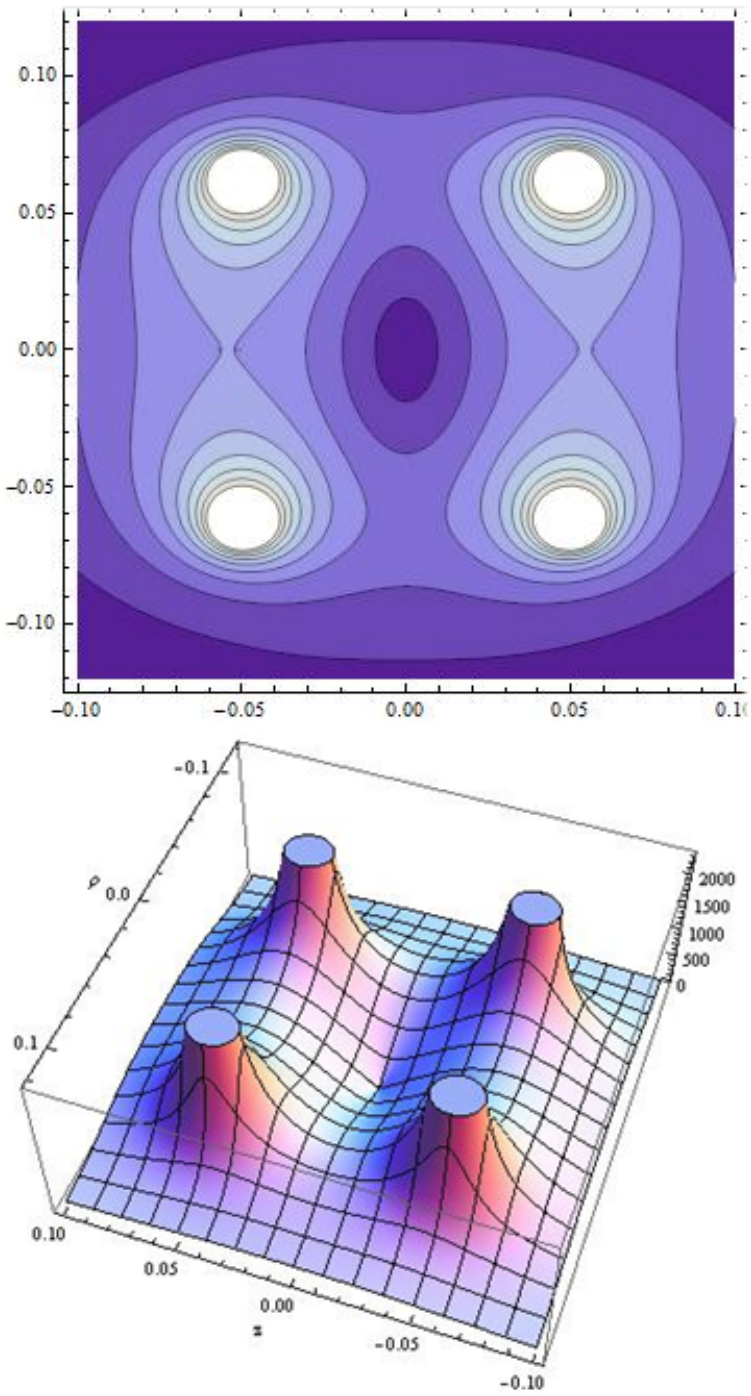

Figure 3.10: The calculated plot of the magnetic quadrupole field

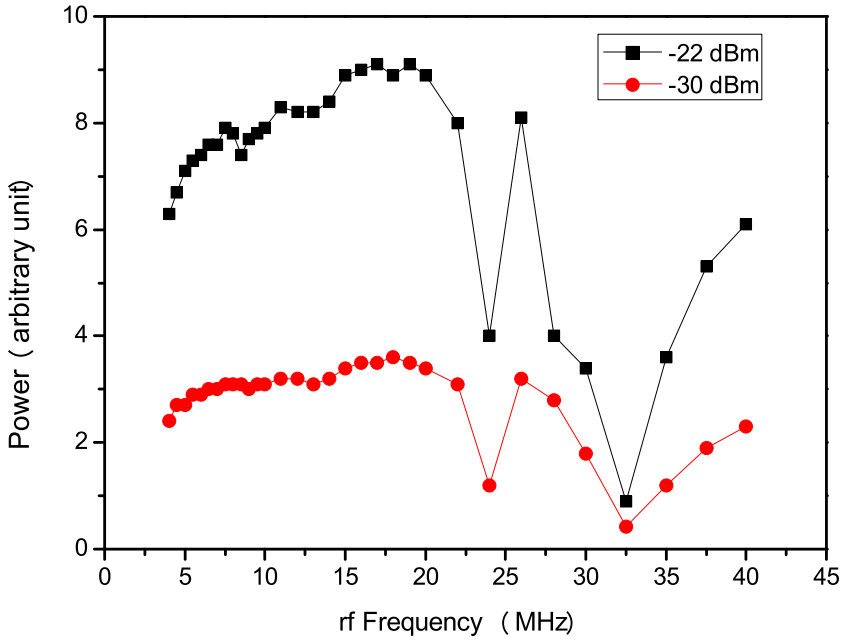

Figure 3.11: The measured rf power.

3.5 Rf Circuit

The evaporation coil pair has Helmholtz geometry with two turns and it has a diameter of 6.5cm. The rf current is created by a DS345 signal generator and the rf signal is amplified by an rf amplifier(ZHL-5W-1, MINI Circuit) and it is switched by a switch(ZFSW-2-46, MINI Circuit). The power of the radio-frequency evaporation field is measured by a pick-up coil or by-pass voltage measurement(Fig. 3.11). The rf power is changed with varying the frequency, the power is also controlled at each frequency for preventing the rf power broadening as possible.

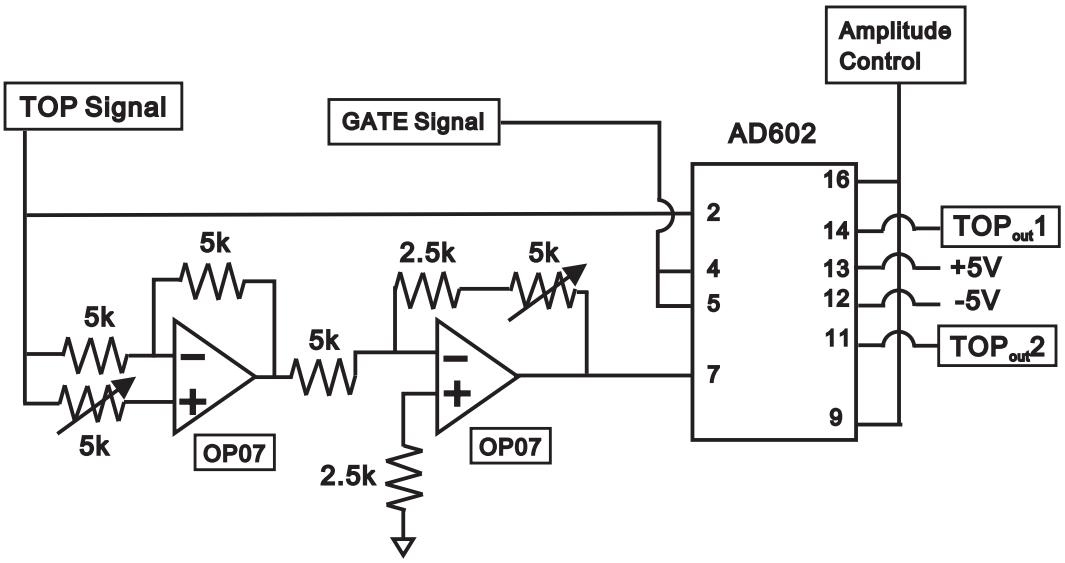

Figure 3.12: The control circuit of the TOP bias field

3.6 Time averaged Orbiting Potential(TOP) Field

The TOP bias field supplying system is consisted a function generator, a control circuit, an audio amplifier, transformers and two pair of Helmholtz coils. A sine signal is produced by a function genarator(DS335). The control circuit divide the generated signal into two sine signals whose phase is different 90 degree. The control circuit also control the amplitude and switch the signals by the computer program. The circuit diagram is shown at fig.3.12 .The transformer is for impedance matching between the coils and the audio amplifier. The bias signal is $7kHz$ in the experiment, the frequency is well matched the operating range of an audio amplifier.

Analog Port	Parameter	Digital Port	Parameter
A_{out} 0	2nd Trap Amp.	D_{out} 0	1st Trap Shutter
A_{out} 1	2nd Trap Freq.	D_{out} 1	2nd Trap Shutter
A_{out} 2	rf switch	D_{out} 2	Repump Shutter
A_{out} 3	Repump Amp.	D_{out} 3	Push Shutter
A_{out} 4	Push/Probe Amp.	D_{out} 4	IPM switch
A_{out} 5	Coil Current	D_{out} 5	Probe Shutter
A_{out} 6	Coil Voltage	D_{out} 6	TOP On/Off
A_{out} 7	Dipole Amp.	D_{out} 7	CCD Trigger
A_{out} 8	TOP Amp.	D_{out} 8	Reserve
A_{out} 9	Push/Probe Amp.	D_{out} 9	Depumper Shutter
		D_{out} 10	Dipole Shutter
		D_{out} 11	CCD Shutter

Table 3.2: The specification of the Analog out and Digital out control by the main experimental computer

3.7 Computer Control System

As the most experiments in now, we control the most experimental parameters by computers. Two computers are used for the experiment, one is the control computer with FPGA(field programmable gate array) and AO/DO board and the another is for using the CCD camera and obtaining the image of atoms. We use the Lab-view as a programming language that is very easy to coding and debugging. The FPGA has its own $40MHz$ clock, the control signal could be generated every $5\mu s$. The out port and the control parameters are shown at the table.3.7. The TTL control signal and the laser intensity measured by a photo diode are shown at the Fig.3.13, it is represent the response time and shutter working time.

The lasers are turned on and off by a mechanical shutter and a AOM.

The mechanical shutter is controlled by the TTL - digital out signal and the AOM is controlled by the analog signal. The mechanical shutter block the laser perfectly but the response time is longer than the response time of the AOM control. The response time of the mechanical shutter and the AOM are shown at Fig.3.13 and Fig.3.14. The response time of the mechanical shutter is 1.2 $1.5ms$ and the shutter closed within $1ms$. The AOM respond less than $10\mu s$ after turn on the analog switching signal.

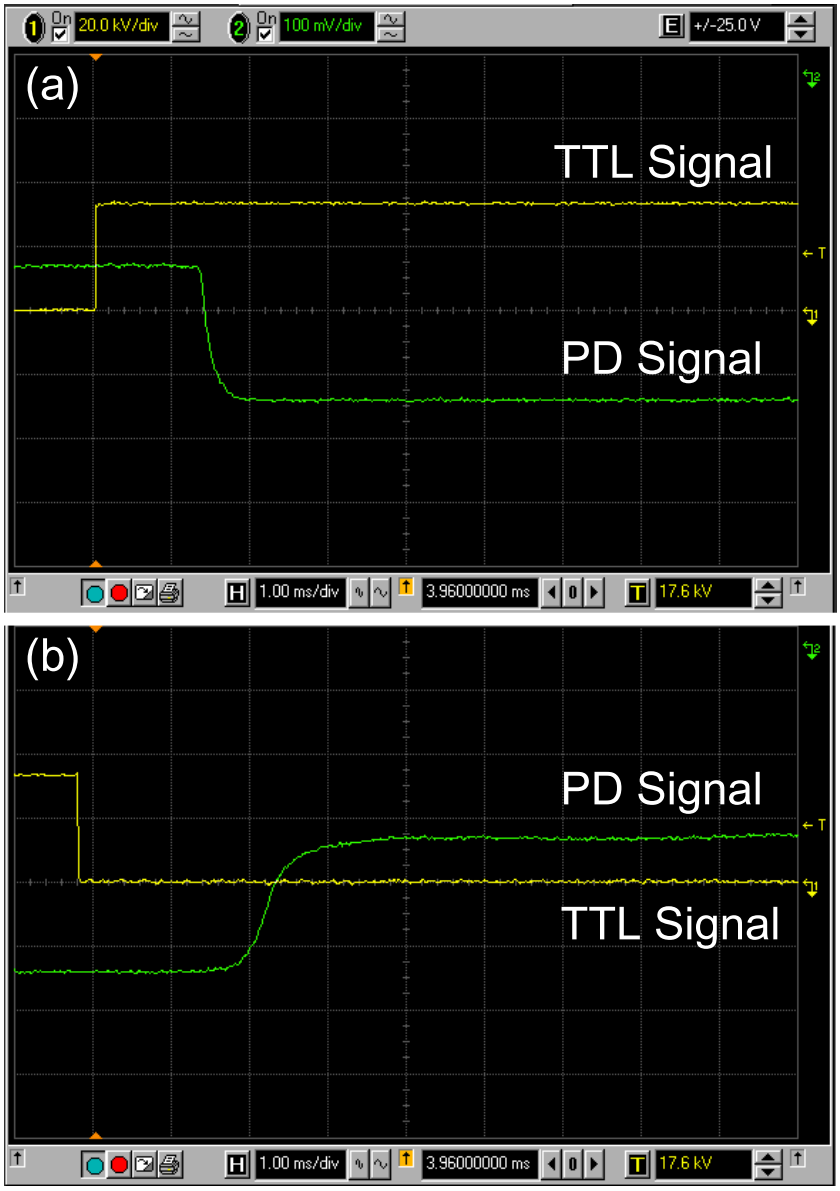

Figure 3.13: Measurement the response of a mechanical shutter. (a) The shutter is switched off and the response time is 1.3 ms and closed fully with 0.4 ms (b) Switched on. The response time is 2 ms and it open within 1 ms.

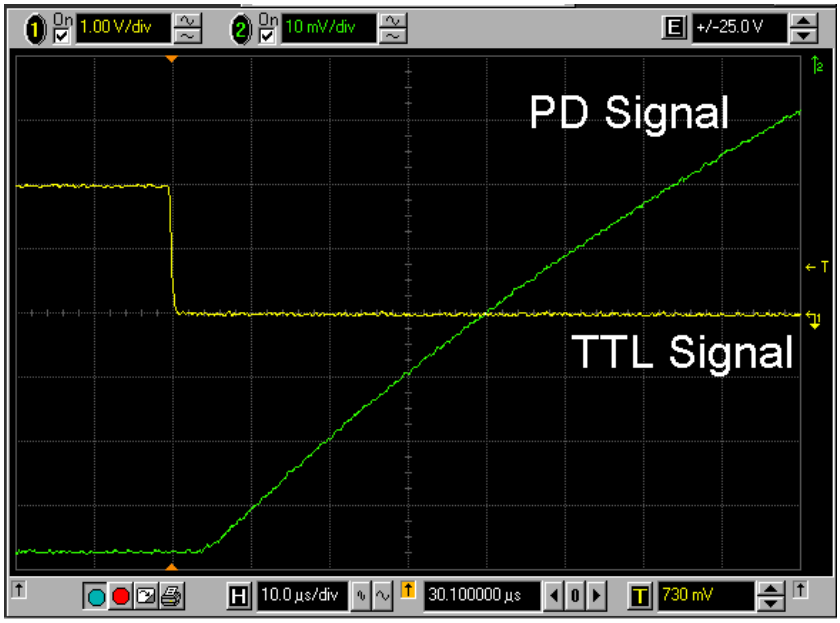

Figure 3.14: A measurement result of turn off the lasers with a AOM, the PD signal is inverted. The response time is about 5 μs.

Chapter 4

Result and Analysis

4.1 Imaging and Analysis

There are two main probing technique to detect trapped atoms in our experiment, one is fluorescence imaging method and the other is absorption imaging method. The magneto optically trapped atoms are easily detected by PD(Photo-Diode), CCD(Charge Coupled Device, Pixel Fly QE, PCO.) and eyes due to the fluorescence light from the atoms. The number and loading time of the magneto optically trapped atoms are obtained by fluorescence imaging method that is composed an aperture, an imaging lens system and a PD or CCD. A schematic diagram of the fluorescence imaging system using PD is shown at Fig.4.1 . We detect the fluorescence light from the atomic cloud passing through an imaging lens system by a PD or CCD [46, 89]. The number of trapped atoms is obtained by the following relation

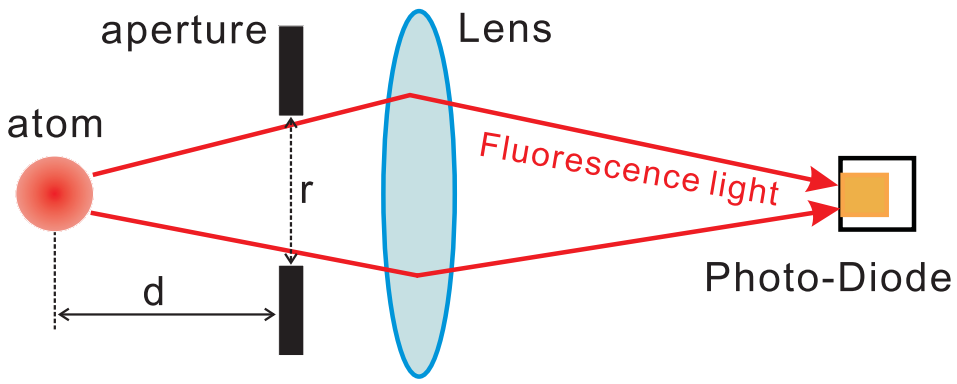

Figure 4.1: A schematic diagram of the fluorescence imaging method. d is the distance from the atomic cloud to the aperture and r is the diameter of the aperture.

$$I \cdot \rho_{PD} = N \cdot \frac{\Gamma}{2}(\frac{s}{1+s})\hbar w \Omega, \tag{4.1}$$

where I is measured current of photodiode, ρ_{PD} is the quantum efficiency of the photodiode, N is the total number of atoms, w is the frequency of the laser and the solid angle of the fluorescence light $\Omega = \pi(r/2)^2/4\pi d^2$, where r is the diameter of the aperture and d is the distance from the atom to the aperture [50]. The fluorescence imaging method is applied to measure number of magneto optically trapped atoms in the first chamber and the second chamber.

Another probing method, absorption imaging, is used for detecting atoms in a pure magnetic potential or a optical dipole potential because there are no fluorescence light from the atoms in that kind of potentials. By shining a resonance laser light to the atoms, the shadow of the atomic cloud can be detected. The absorption imaging method use the resonance light, the initial status of the atoms - the temperature, the momentum, the state of the atoms and so on - are destructed by the imaging process. A schematic diagram of the

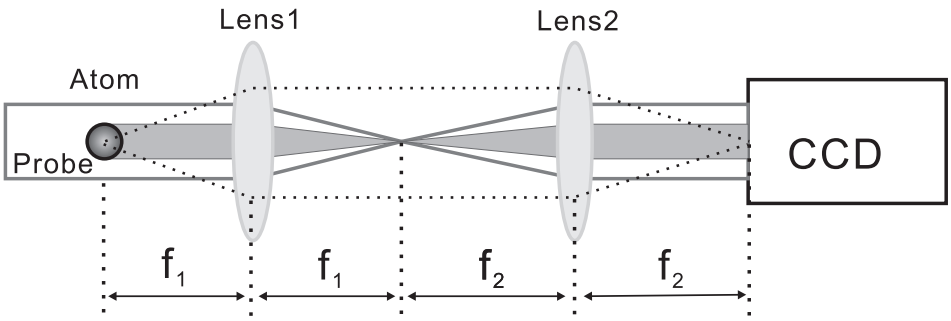

Figure 4.2: A schematic diagram of the absorption imaging method. f_1 is the focal length of the lens1 and f_2 is the focal length of the lens2.

absorption imaging system is shown at Fig.4.1.

The lens1 is located at the distance of its focal length f_1 from the atoms, and the lens2 is located at the distance $f_1 + f_2$ from the lens1 where f_2 is the focal length of the lens2. The CCD is at the distance f_2 from the lens2 for detecting the fluorescence light from the atoms and the probe shadow by the atoms both. The position of the CCD is decided while imaging the magneto optically trapped atoms. The magnification of the imaging is simply f_1/f_2.

The probe laser passing through atomic cloud is attenuated exponentially via the optical depth(OD). It is known as Beer's rule [90] that is

$$I_{abs} = I_0 \cdot e^{-OD}, \tag{4.2}$$

where I_{abs} is detected probe image with the shadow of atoms and I_0 is the initial probe light. Practically we take three shots to obtain the optical depth that is related value with the density of the atomic cloud.

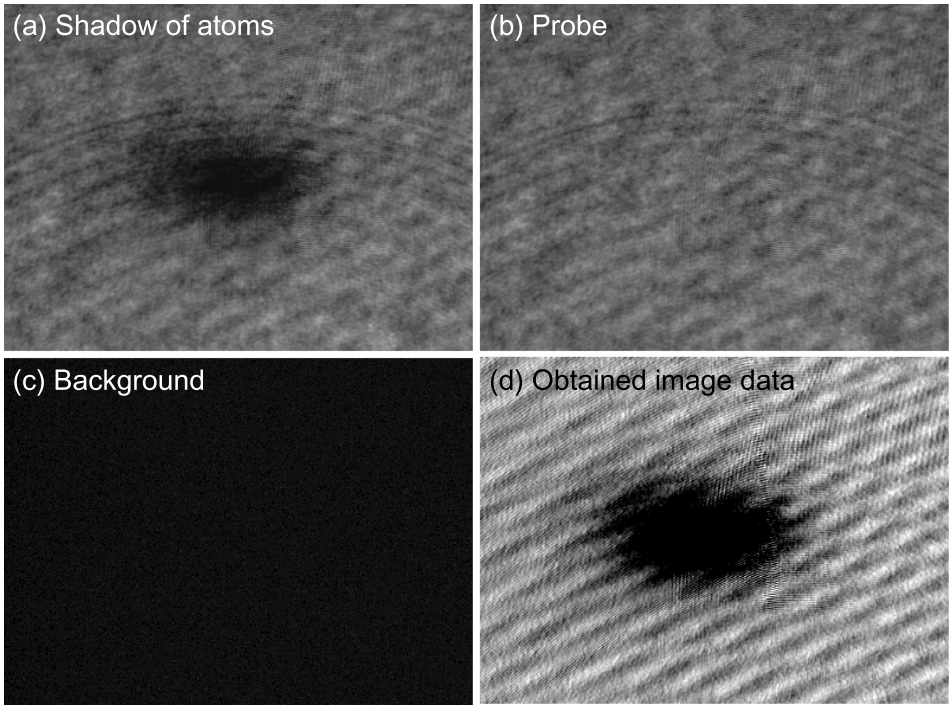

Figure 4.3: Sample absorption images of the magneto optically trapped atoms. (a) A shadow image of atoms with probe laser. (b) An image of the probe laser only. (c) An image of Back-ground without any lasers. (d) An obtained image data from the three(a c) images.

$$OD = ln[\frac{I_{abs} - I_{bg}}{I_0 - I_{bg}}]. \tag{4.3}$$

I_{bg} is a background image taken without any probe light and atoms. A sample absorption image of magneto optically trapped atoms is shown at Fig.4.1.

The number of atoms is measured from the absorption image by the integrate column density or Gaussian fitting. The each value of CCD pixel is related to the column density of the atoms and the column density is obtained by

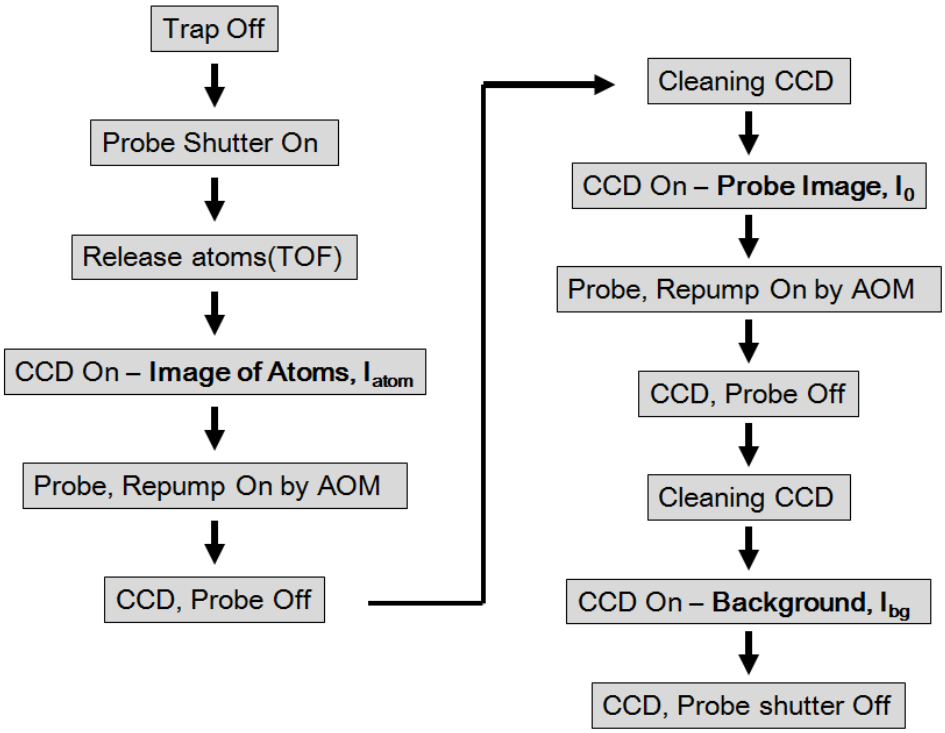

Figure 4.4: Diagram of imaging procedure. The probe laser is controlled by AOM for fast switching. The 3 images are obtained in the imaging process.

the simple equation of OD/A, where the absorption cross-section A is expressed as follows [89];

$$A = (\frac{\Lambda}{2})(\frac{3\lambda^2}{2\pi})\frac{1}{1+4\frac{\delta(r)^2}{\Gamma^2}}, \tag{4.4}$$

where λ is the wavelength of the transition, the detuning $\delta(r)$ is a function of the distance r from the trap center, and the branching ratio Λ for the F=2 to F′=3 transition at the linear polarization beam is 7/3 in our case. The absorption cross section is effected by detuning changed due to the magnetic field [91], the magnetic field have to be concerned at in=-situ imaging.

The number measurement by integrating CCD pixel is very simple and fast method but it has two problems due to the bad pixels and saturation. These errors could be solved by introducing the gaussian fitting of the whole image.

The density distribution of the atomic cloud is well matched the Gaussian distribution. When the trap is switched off, the trapped atoms fly ballistically at their velocity. For an atom starting at point r_0 to arrive at a point r after a time t, integrating over all initial positions r_0 the density distribution is given by,

$$n_{tot} = \frac{1}{h^3}\int d^3r_0 d^3p \frac{1}{e^{-(\mu - H(r_0,p))/k_BT)} - 1}\delta^3(r - r_0 - \frac{pt}{m}) \tag{4.5}$$

$$= \frac{1}{\Lambda_{dB}^3}\prod_{i=1}^{3}(\frac{1}{1+w_i^2t^2})g_{3/2}(exp[\mu - \frac{m}{2}\sum_{i=1}^{3}x_i^2(\frac{w_i^2}{1+w_i^2t^2})]). \tag{4.6}$$

Where, w_i is the trap frequency, the de Broglie wave $\lambda_{dB} = (2\pi\hbar^2/mk_BT)^{1/2}$ and the Bose function is given by $g_j(z) = \sum_i z^i/i^j$. At large times ($t \gg w_i^{-1}$),

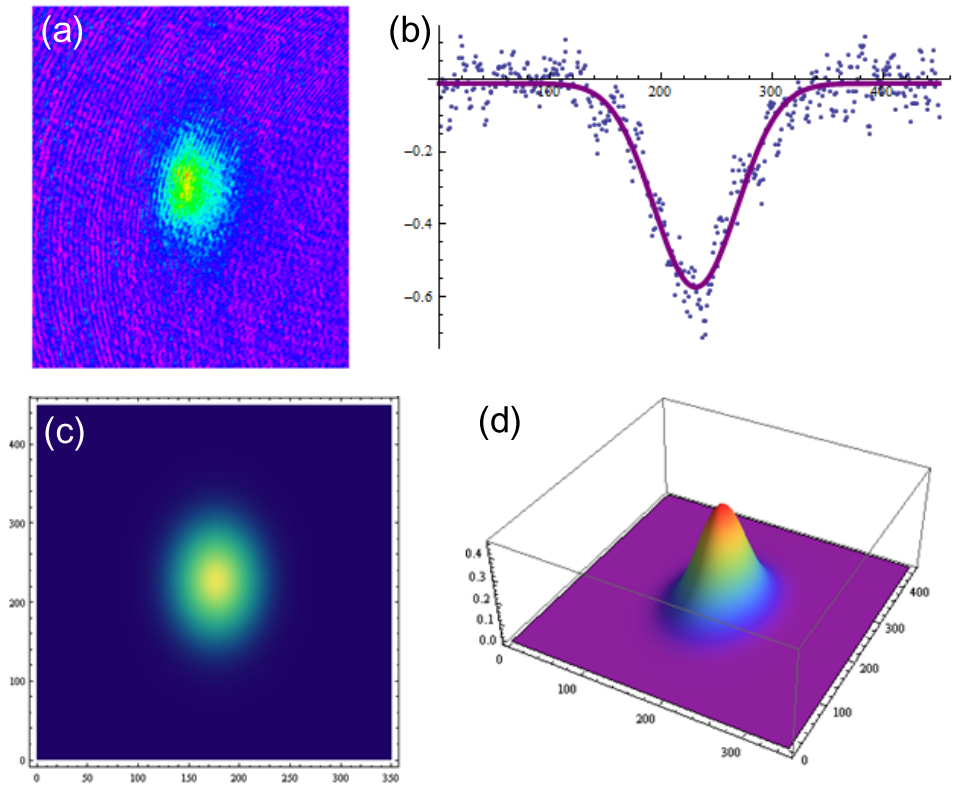

Figure 4.5: The obtained image(a) of atoms are fitted as a Gaussian profile of 1D(b), 2D(b) and 3D(d) for obtaining atomic properties.

the density profile becomes,

$$n_{TOF}(r,t) = \frac{1}{\lambda_{dB}^3} g_{3/2}(e^{(\mu - \frac{mr^2}{2t^2})/k_B T}). \tag{4.7}$$

The Gaussian fitting of an image of atoms are shown at Fig.4.1. The obtained image is fitted as a 1D, 2D and 3D Gaussian distribution.

If the trapped atoms are dense enough to absorb the probe laser, the obtained optical depth(OD) is less than the real value due to the saturation. In that case, the image fitting is not exact to the original one, only the tale of the

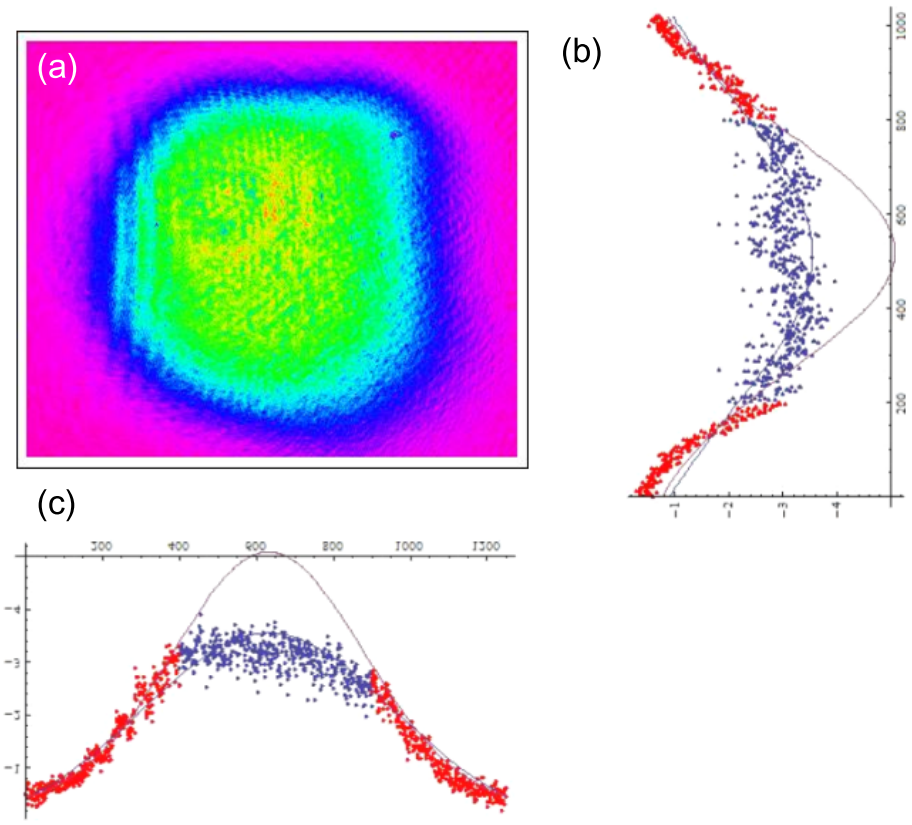

Figure 4.6: The saturated image of atoms are fitted from its tale.

image is fitted to the Gaussian distribution. The fitting sample is shown at the Fig. 4.1.

The temperature of atoms are measured by release and recapture method, time of flight(TOF) and in-situ imaging in generally.

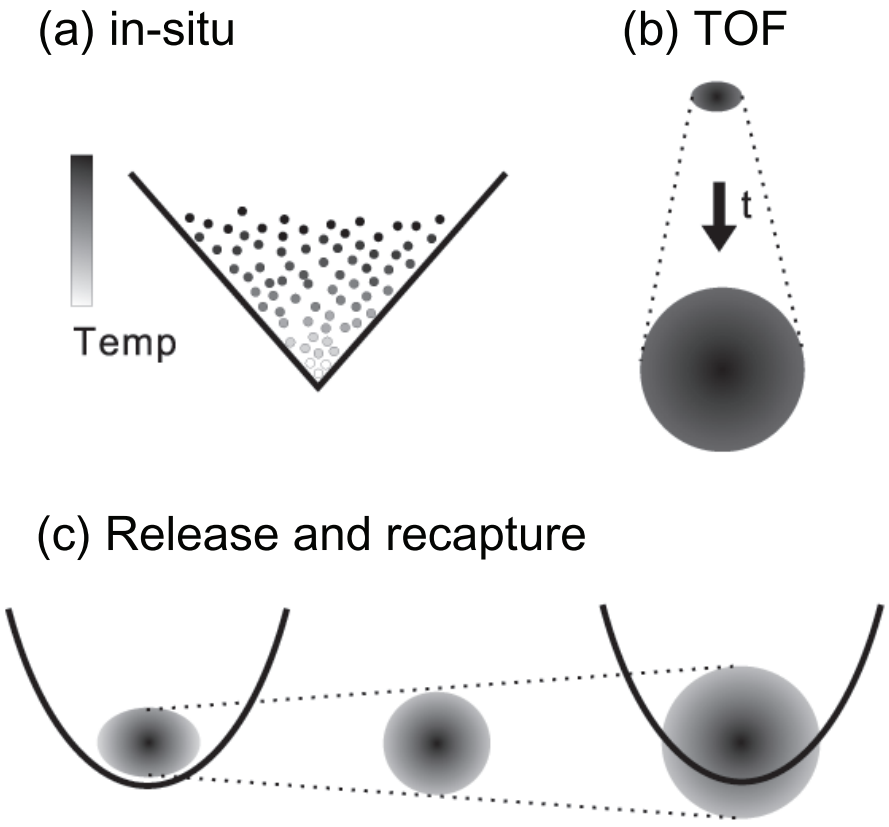

Figure 4.7: Methods of temperature measurement. (a) Temperature measurement by the size of atoms of in-situ imaging for thermal gas. (b) Time of Flight(TOF) method : The distribution of atoms after free-fall in time t is related on the temperature of cloud. (c) Release and recapture : The ratio of trapped atoms between initially trapped atoms and trapping after expand.

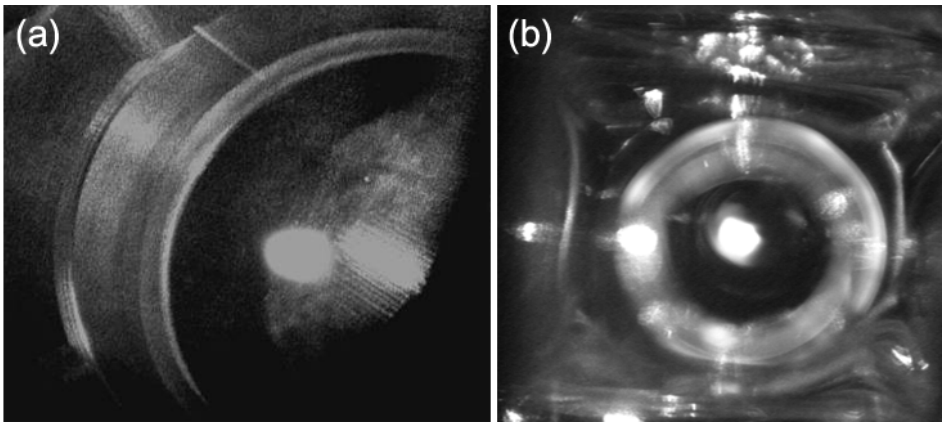

Figure 4.8: Photos of the magneto optically trapped atoms at the first chamber and the second chamber.

4.2 Magneto Optical Trap

The first step of the experiment is magneto optical trap(MOT) at the first chamber which is a atom source. For fast and enough supplying cold ^{87}Rb atoms to the 2nd glass chamber, it is necessary to capture large number of atoms and to have fast loading rate at the first chamber. A photo of the magneto optically trapped atoms in the first chamber is shown at Fig.4.2(a) and in the second chamber is shown at Fig.4.2 (b).

The trap laser intensity of the 2nd chamber is $2mW/cm$ and the detunning is -2.5Γ. The magnetic field gradient is $20G/cm$. The number of the atoms in the first chamber is over 1×10^{10}, that value depends on the trap laser intensity and the amount of the Rb gases from the getters. The Rb getters in the vacuum chamber is attached at feed through by spot welding. The number is measured by fluorescence imaging method. Typically, the most important condition of trapped atoms in the first chamber is the loading time as a atomic

gas reservoir rather than the number of atoms. The loading time in the first chamber is maintained less than 1 s during the experiments.

The trapped atoms in the 1st chamber are transferred by the laser pushing process. The detunning of the push laser is -3Γ and the transfer time is about $3s$ typically though it depends on the various trap conditions. The pushing efficiency at each detunning is shown at Fig.4.2 (a) and the measured fluorescence light of 2nd MOT loading is shown at Fig.4.2 (b).

The trapped atoms in the 2nd chamber after a few seconds pushing process from the 1st chamber are observed by the fluorescence imaging method and the absorption imaging method. The obtained number by the absorption imaging is calibrated with the fluorescence imaging. A typical image of the magneto optically trapped atoms in the 2nd chamber is shown at the Fig.4.2.

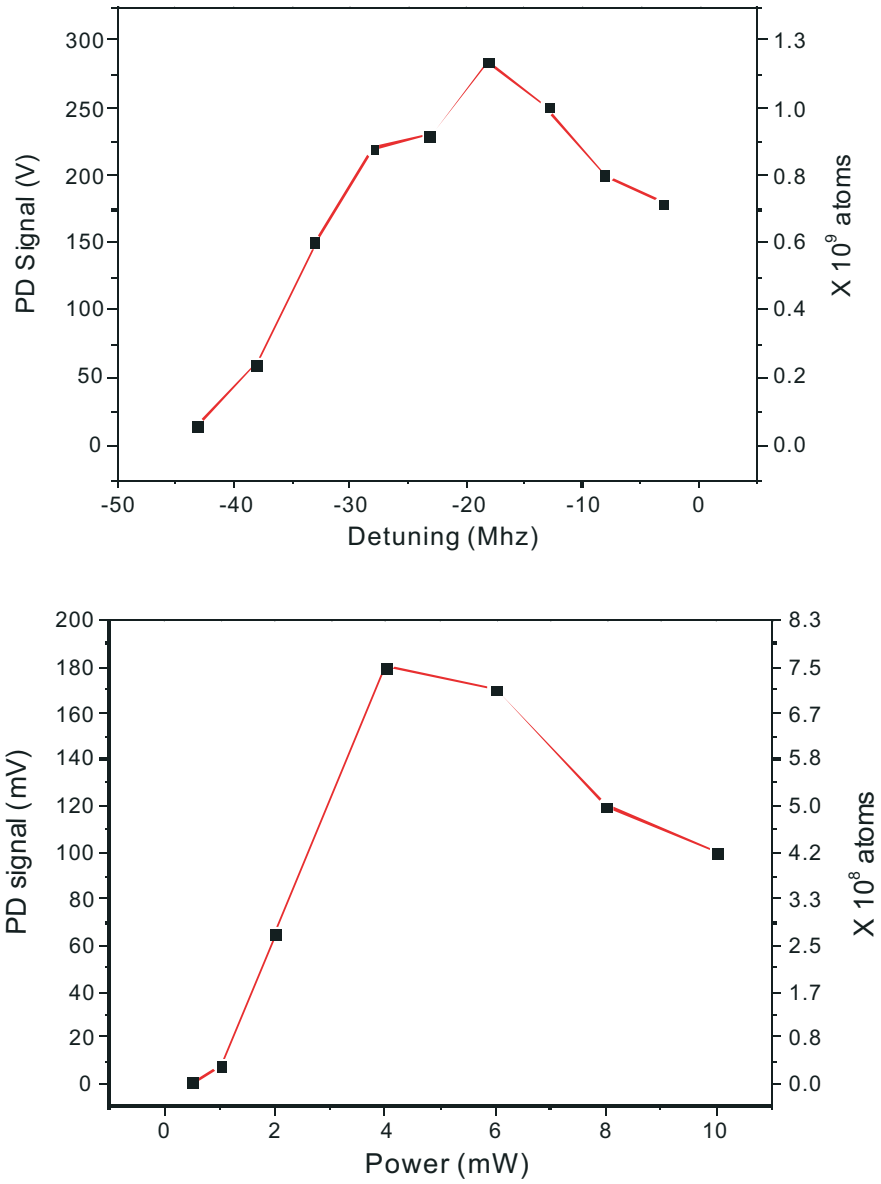

Figure 4.9: Measurement of pushing efficiency. The fluorescence light of the atoms in the 2nd chamber was measured by a photo diode with varying (a) pushing laser detunning or (b)power of pushing laser.

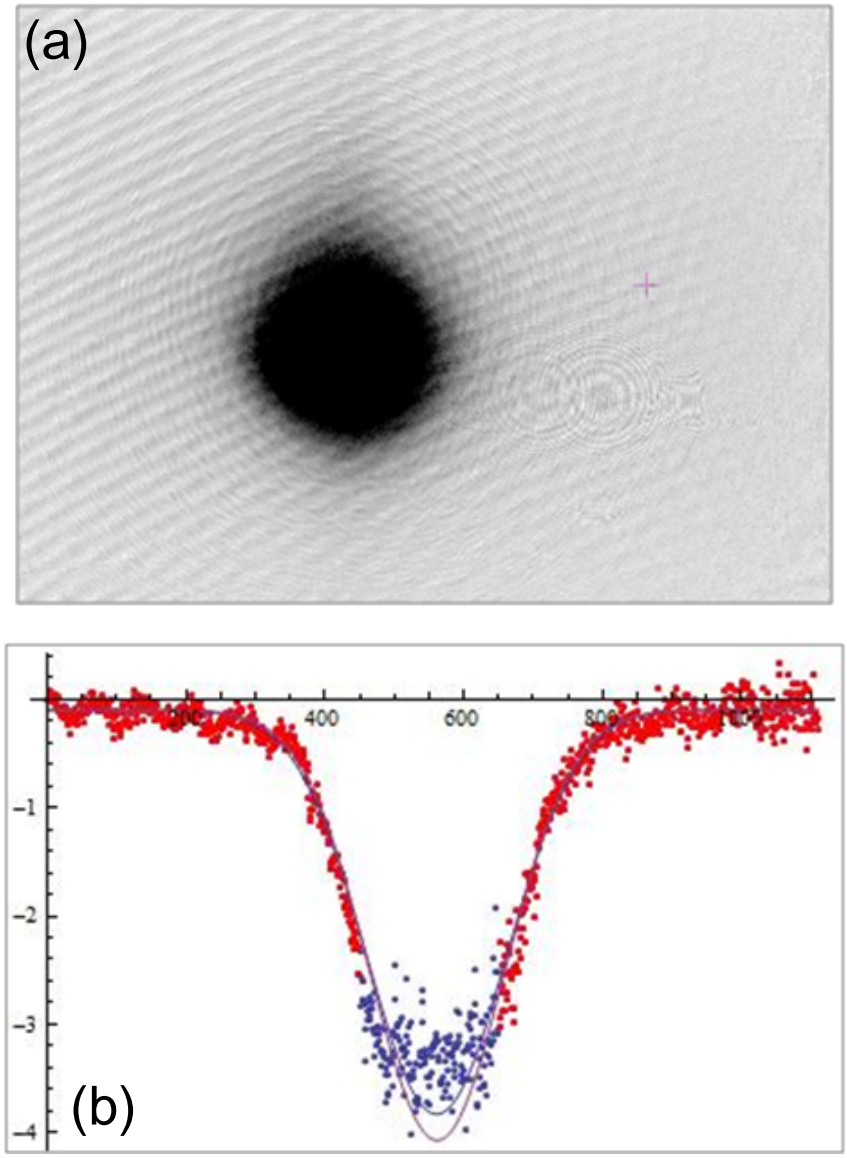

Figure 4.10: (a) A typical absorption image of the magneto optically trapped atoms in the 2nd chamber and (b)its profile.

4.3 Pre-cooling Stage

4.3.1 Compressed MOT

The next step is compressed-MOT(cMOT) after magneto optical trap. There are two main reasons doing the cMOT stage. First, the density of trapped atoms is increased more than the MOT stage [92, 93]. Second, the position of the atomic cloud moves closer the center of the magnetic field gradient that is zero value of the magnetic field. The atomic position is very important to catch it magnetically, i.e. magnetic spherical quadrupole trap or TOP trap.

In cMOT stage, the detunning of the trap laser and the magnetic field gradient are increased. The detunning is 4Γ and the magnetic gradient is increased from $20G/cm$ to $75G/cm$ within a few ms. The compression time is chose the shortest time not to occur oscillatory motions of atoms after loading in a magnetic trap. When the compression time is less than 5 ms, an oscillatory motion or excitation is observed in magnetic trap which is mentioned next subsection.

The number of atoms in the compressed MOT does not changed compare with the number in a MOT before, but the density is increased by a factor 2 due to the experiment parameters.

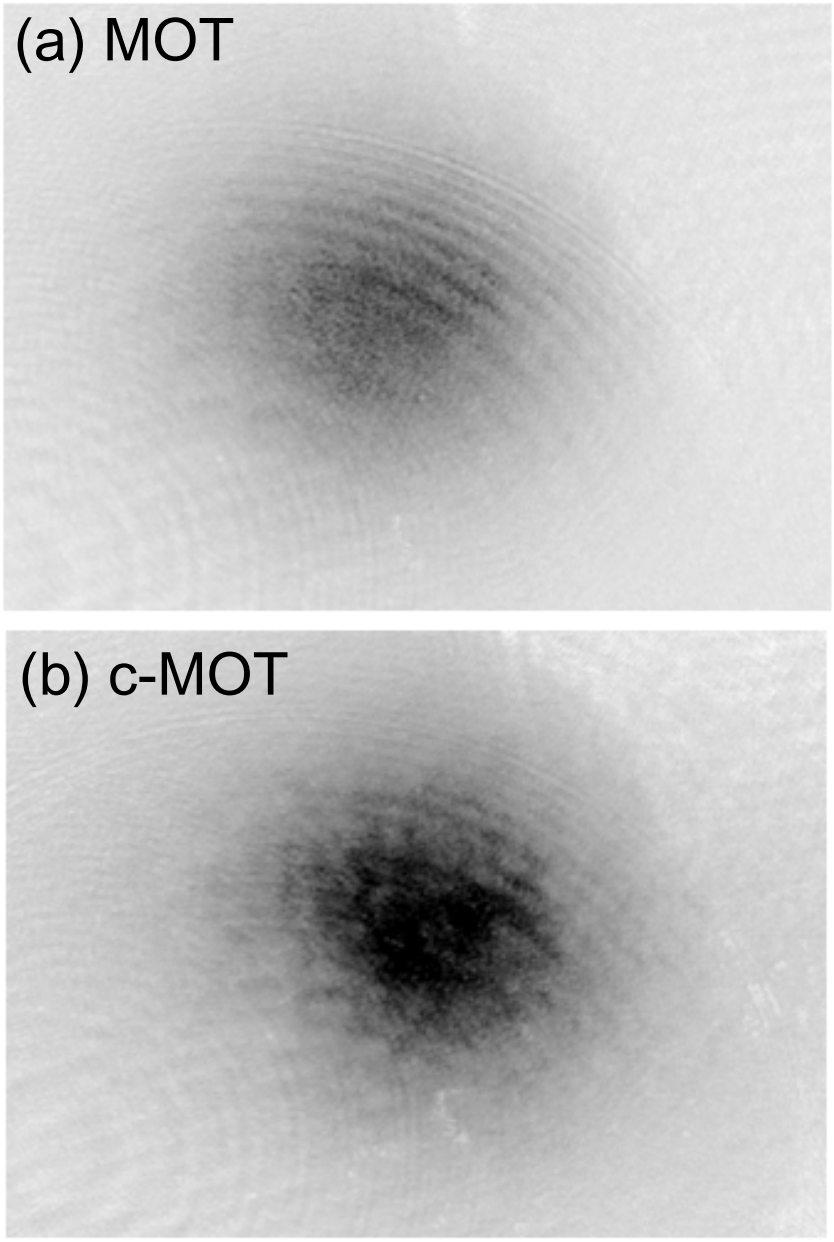

Figure 4.11: Absorption image of atoms in (a)a MOT and (b)a cMOT. The two images are contrasted with optical depth of 2. The density of atoms in a cMOT is lager than in a MOT.

4.3.2 Oscillatory motion in a magnetic trap induced by a compressed MOT

The atoms are compressed by increasing magnetic quadrupole gradient during the cMOT stage. The strength of z-direction quadrupole field gradient is twice than the longitudinal direction, the compressing force is twice also. If the rethermalizing time is not enough, the atoms keep their momentum in the magnetic trap. Thus the short time of a compressed MOT induce the oscillatory motion of atoms in a magnetic trap. This phenomenon is the first observation in my best knowledge. The image of excitation and a preliminary oscillation data are shown at Fig.4.3.2 and Fig.4.3.2.

The mechanism of creating the oscillation is guessed as follow. The atoms are compressed in the cMOT stage by the magnetic field and the laser field. For the magnetic field, the field gradient of z direction is twice than the longitudinal direction and the atoms are forced twice along z direction. The lasers acts a damping force to the atoms in the magneto optical trap, the atoms are rethermalize in the laser light field. However if the compressing time is less than 5 ms, the compressed atoms does not forced by laser field, the atoms have a momentum along the z direction. Thus the atoms oscillate in the magnetic trap in which there are no damping force. The oscillatory motion is observed during a few seconds. The oscillation results can be a detecting method to measure the trap frequency that is the magnetic field gradient.

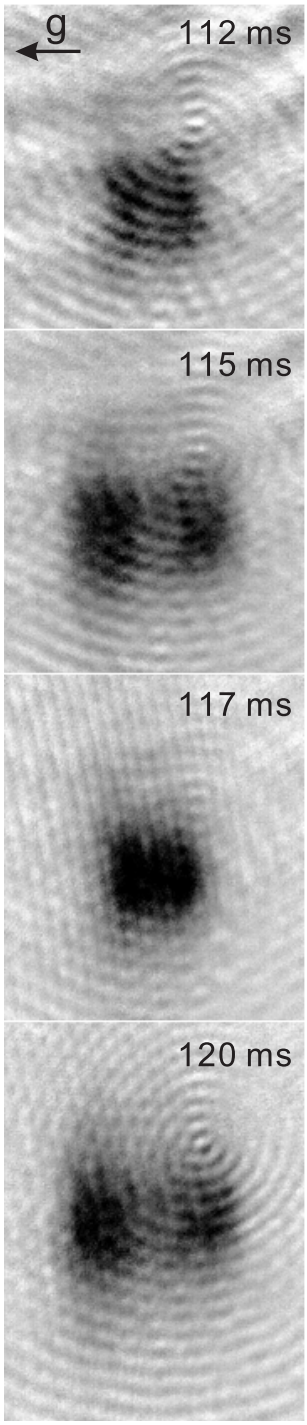

Figure 4.12: Oscillatory motion of atoms in a magnetic quadrupole trap induced by a short time cMOT

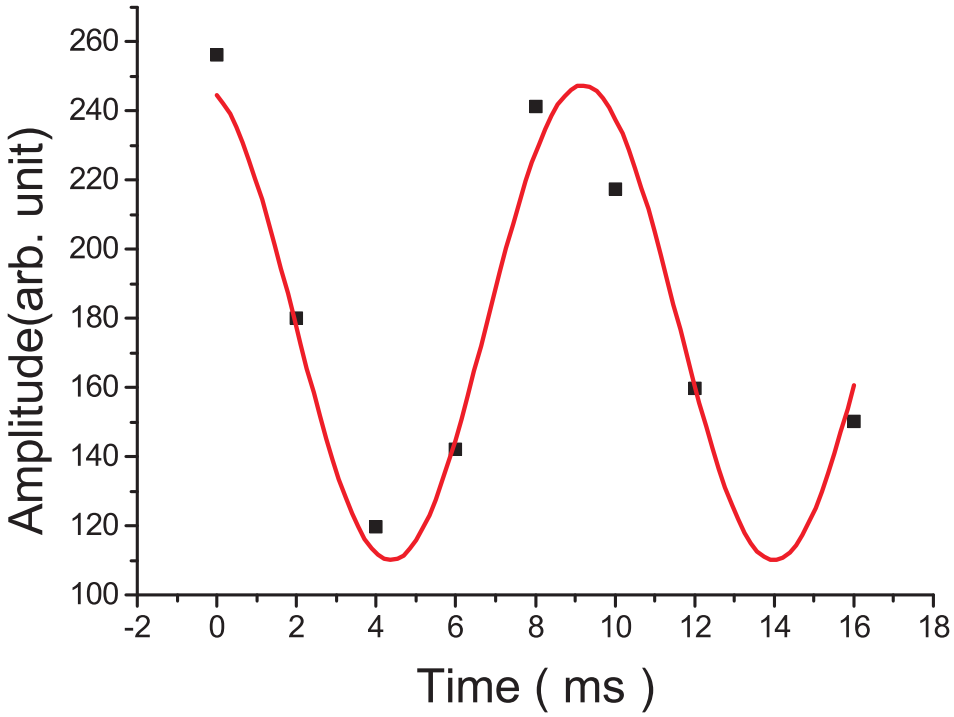

Figure 4.13: The oscillation of motion is fitted as a sine curve. The oscillation frequency is about 100 Hz.

4.3.3 Optical Molasses Cooling

The Doppler limit was understood as a limit temperature of the laser cooling for the detuning is equal to the $\Gamma/2$. But when the laser detuning is larger, the temperature of atoms is lowered below the Doppler temperature and it was understood as a sysiphus cooling(or molasses cooling) [94] [95] [96].

When an atom is in the propagating linear polarized laser light, the atomic state is separated due to the interaction with the laser field named AC stark shift. The polarization of laser field changes with z for depending on the polarization of incident beam. In the spacial distributional change of laser light field, the atomic state is varying with the field. In a certain velocity of atom, the state selective absorption and emission make the energy difference below doppler limit between loosing and gaining momentum.

In the molasses cooling stage, the laser detuning is increased from 4Γ to 10Γ and the intensity is lowered to $1mW/cm^2$ without magnetic field gradient [13]. In a molasses cooling process the temperature is proportional to the intensity and inverse of detuning.

$$T \propto \frac{I}{\delta} \tag{4.8}$$

Thus the temperature is lowered when the intensity is decreased and the detuning is increased. The temperature measured by TOF image and obtained about $10\mu K$4.3.3. However the temperature of atoms is lowered by the molasses cooling, switching magnetic field gradient make the loading efficiency in

magnetic trapping lowered when it turned off. In the experiment, the magnetic field did not turned off and only the laser light field was controlled with optical pumping.

molasses cooling

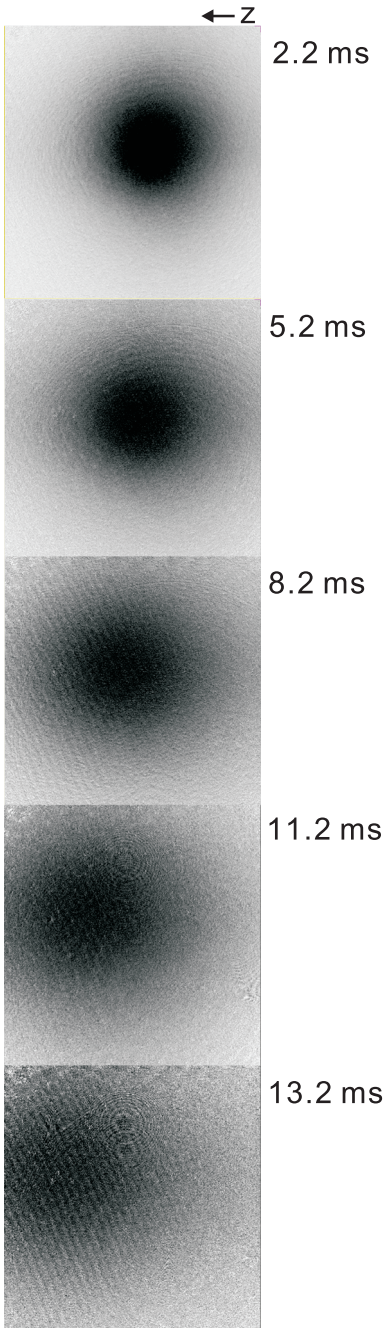

Figure 4.14: A time of flight(TOF) image of atoms after molasess cooling

4.4 Optical Pumping

We use the cycling transition from the $F = 2$ state to the $F^{'} = 3$ state at the MOT or pre-cooling stage. The ground state of the atomic state of $F = 2$ has 5 magnetic sub-levels, $m_f = -2, -1, 0, +1, +2$. The possible states to trap magnetically are $m_f = +2, +1$ state that are weak field seeking state. And also there is one more ground state of the ^{87}Rb D2 line that is the $F = 1$ state. In the $F = 1$ state, the weak field seeking state is $m_f = -1$ state.

If the magnetic sub-level of atoms is not one state, for example $|F = 2, m_f = +2 >$ and $|F = 2, m_f = +1 >$, the evaporative cooling efficiency is decreased because the atoms that have different temperature are in the same depth of potentials due to the difference of magnetic moment. For the magnetic trapping, it is necessary to choose one magnetic sub-level.

The magnetic sub-level is transferred with resonant laser named optical pumping. The $|F = 1, m_f = -1 >$ state is used in the experiment due to the easy pumping process. The trap line $F = 2$ to $F^{'} = 3$ is cycling transition, however the probability of the transition to $F^{'} = 2$ is not zero. Unless the repump laser is in the laser cooling, the atoms are pumped to ground state of $F = 1$. In the experiment, a depump laser $F = 2$ to $F^{'}$ is also used for fast optical pumping [97].

After pre-cooling stage, the repump laser is turned off and de-pump laser is turned on which is the optical pumping stage. The fluorescence light of atoms are observed by a CCD for measuring pumping time, the atoms are on the $F = 1$

ground state less than $1ms$. The optical pumping is checked also by absorption imaging. The atoms are not observed after optical pumping by a probe laser resonant on the $|F = 2>$ to $|F^{'} = 3>$ only. But imaging with a repump laser, the image of atoms could be obtained by probe process(Fig.4.4).

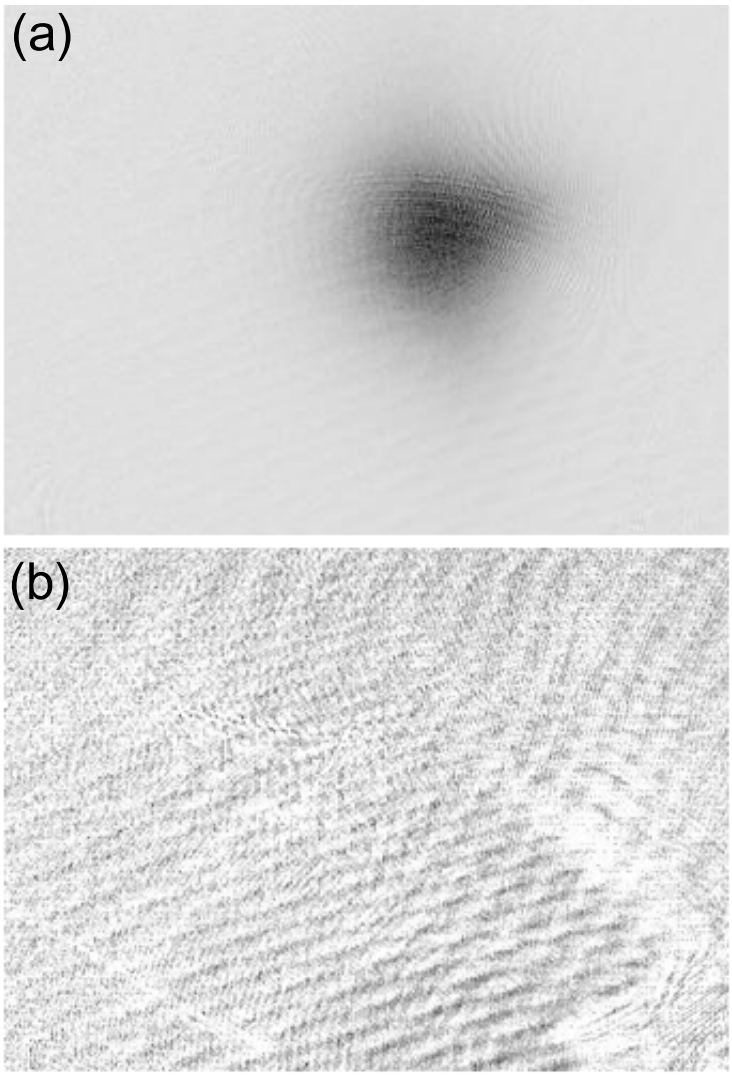

Figure 4.15: An image of the atoms after 2 ms optical pumping process. The absorption image is taken after holing 100 ms in the magnetic trap. (a) An optical pumping image with repump light and (b) without repump light. The atoms are in the $|F = 1 >$ state, the probe light($|F = 2 > \rightarrow |F' = 3 >$) is transparent with the optically pumped atoms.

4.5 Magnetic spherical Quadrupole Trap

As discussed above at chap.2, the MOT or the trapping method based on the resonant light force have limitations to lowering the temperature of the atoms so called Doppler limit or recoil limit. It is needed to trap without resonant light for lowering the temperature below the limitations, the magnetic trap or the optical dipole trap become the general solutions. The magnetic spherical quadrupole trap is one of the most easy way of the variety magnetic trapping method.

At the experimental conditions, the depth of the magnetic trap potential is about one hundred μK which is over the temperature of the molasses cooling. After pre-cooling stage, all the lasers are switched off and the magnetic field gradient is increased to trap the atomic cloud. The trapped atom number at several field gradient values are shown at fig.4.5.

The properties of the trapped atoms in the magnetic quadrupole trap are obtained by the absorption imaging method that is discussed above. The first character is the number of atoms that is measured by a integrating analysis or the gaussian fitting in the experiment. The *in-situ* absorption image of the trapped atoms in the magnetic spherical quadrupole potential and its vertical and horizontal profile are shown at Fig.4.5.

The atom number of trapped atoms in the magnetic trap(Fig.4.5) is 1×10^8 that is calculated by the Gaussian fitting. The integrating method is more fast method than the fitting to obtain the atom number, it is used during

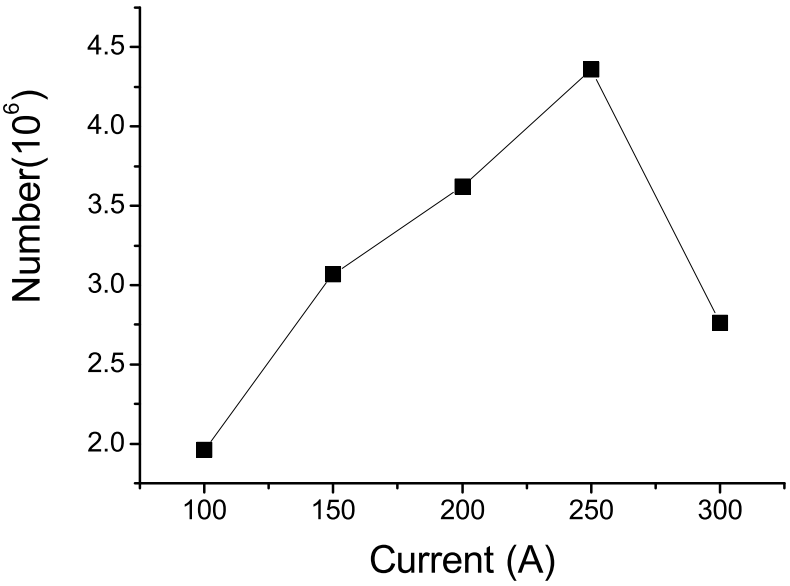

Figure 4.16: The number of trapped atoms in a magnetic quadrupole trap for finding efficiency trapping condition. The number of atoms is maximum at 250 A.

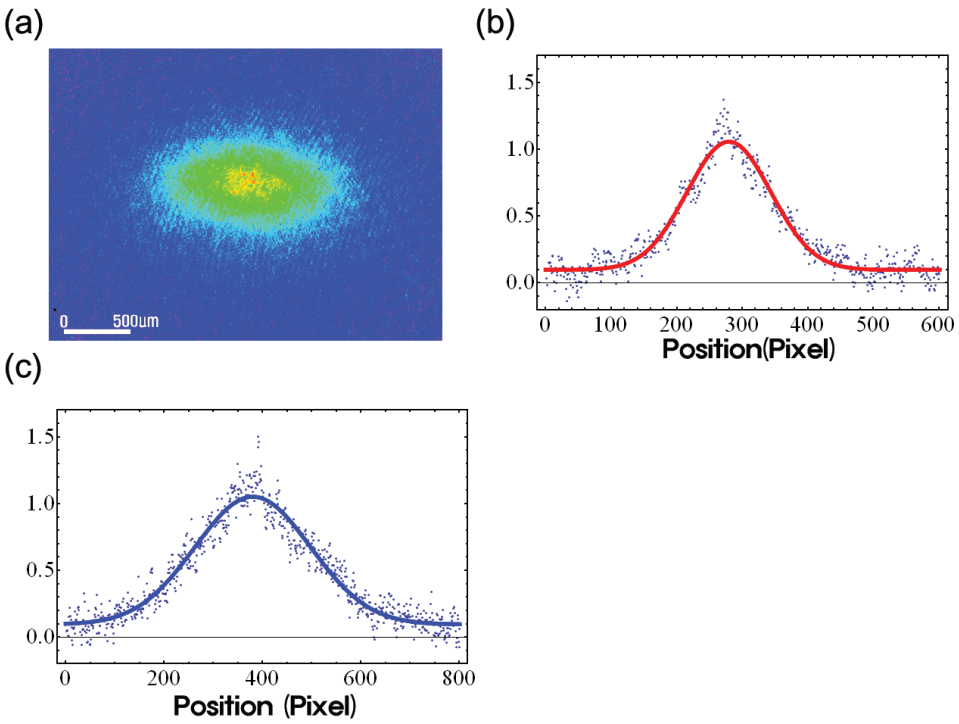

Figure 4.17: (a) An absorption image of the atoms in the magnetic spherical quadrupole trap. The size of scale bar is 500 μK. (b),(c) The profile of the trapped atoms along (b)vertical and (c)horizontal direction.

experiments. But, the integrating method could not correct the errors of the image, i.e. bad pixels, saturated image, the exact properties of the atoms are obtained by the Gaussian fitting.

In a magnetic trap potential, there are several reasons to lose atoms, that are spin flip, scattering with background thermal gas and molecule formation by three body recombination. In the experiment at magnetic quadrupole trap potential, the main reason to lose atoms is the majorana spin flip near the center. The number of trapped atoms is measured at several holding time for obtaining the life-time in the trap. The sample images of atoms in the magnetic trap after trapping few seconds are shown at Fig.4.5 and the life-time is obtained 26 s(Fig.4.5).

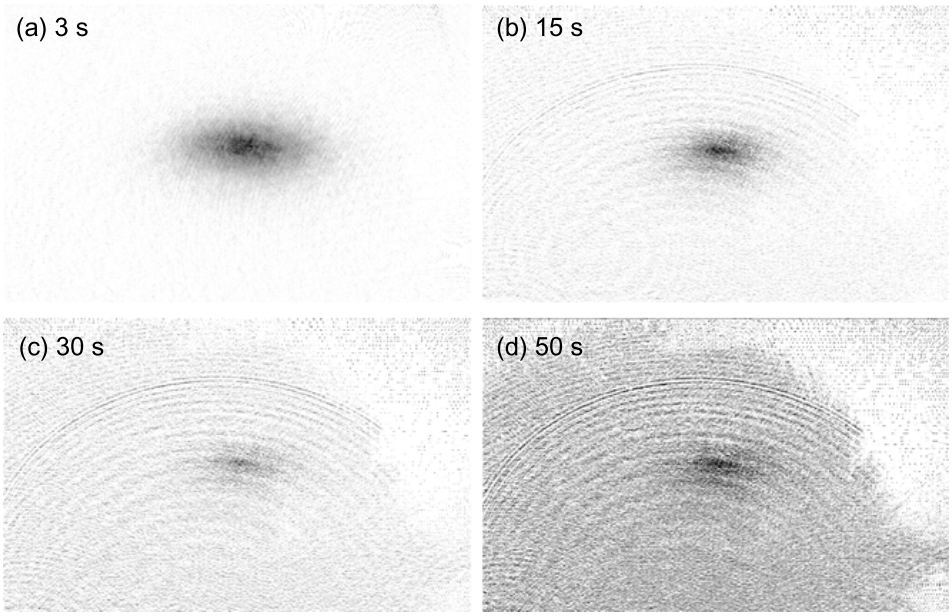

Figure 4.18: Absorption images of atoms in the magnetic spherical quadrupole trap at several holing times. The atoms are in the trap at (a) 3 s, (b) 15 s, (c) 30 s and (d) 50 s.

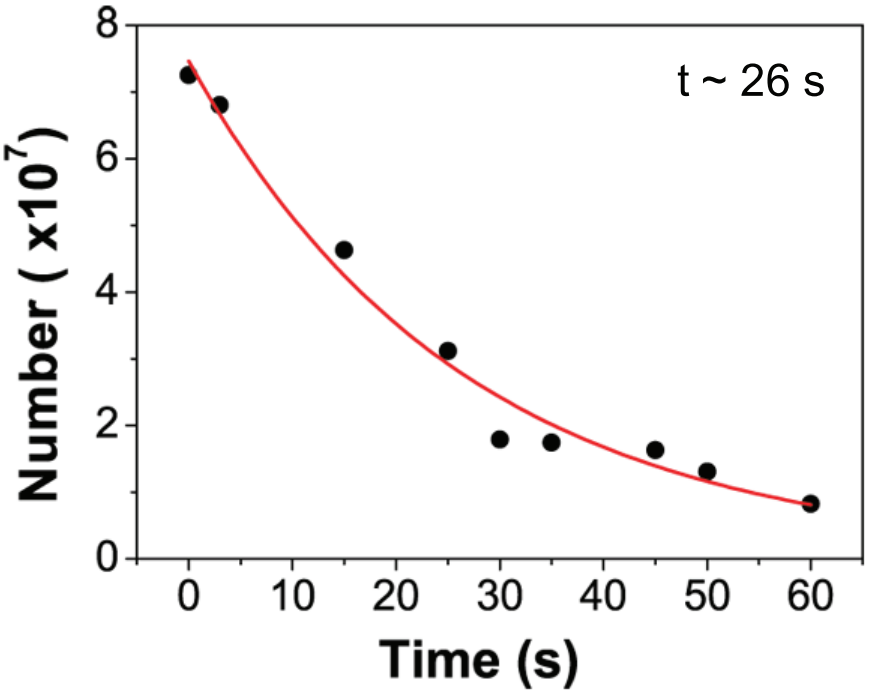

Figure 4.19: The life-time of trapped atoms in the magnetic spherical quadrupole potential. The solid line is a exponential fitting curve and the life-time is obtained 26 s.

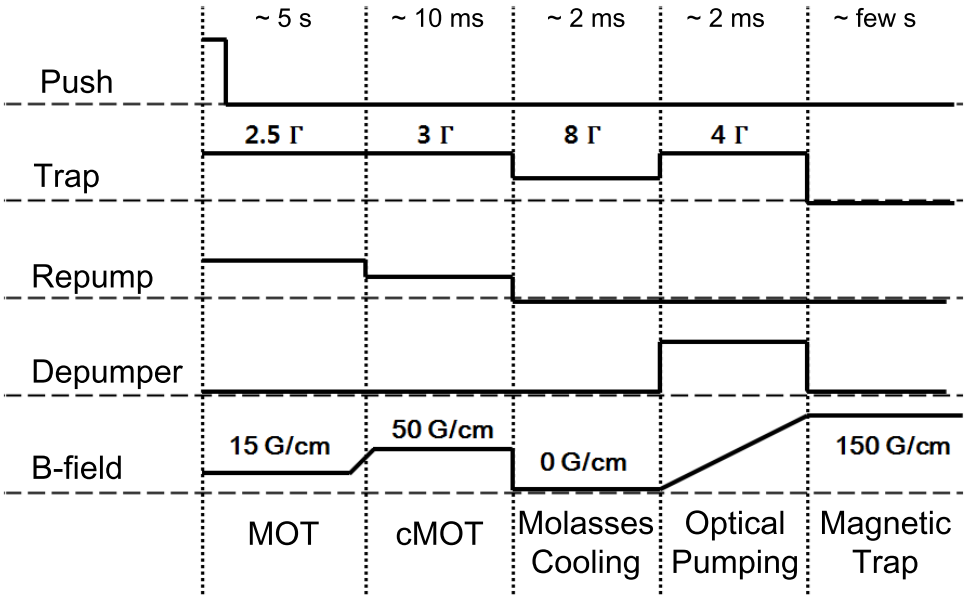

Figure 4.20: Time sequence of the experiment.

4.6 Rf Evaporation

The temperature of trapped atoms in the magnetic quadrupole potential is a few tens of μK that is a hot temperature comparing with the critical temperature of Bose-Einstein condensation. The rf-evaporative cooling is one of the most used way for making ultra cold atoms in a magnetic trap.

We apply radio frequency field resonant on the transition of $m_F = -1$ state to $m_F = +1$, the hotter atoms escape from the trap with hot energy over the average energy. The resonant frequency could be calculated from the Zeeman shift that is given by

$$\triangle E = g\mu_B m_F B^{'} r \tag{4.9}$$

where, g is Landé g-factor, μ_B is Bohr magneton, $B^{'}$ is magnetic field gradient and r is the distance from the center. In the experiment, the typical size of the trapped atoms is about 1 mm (the distance from the center is about $5mm$) at the magnetic field gradient 150 G/cm, the resonance frequency at the edge of the trap is about 10 MHz in the condition [98].

When the atoms are evaporated, the size is decreased and the density is increased. The Fig.4.6 is represent the evaporation works well. A $10MHz$ rf field is applied to the atomic cloud in a magnetic spherical quadrupole trap within $3s$.

The atomic properties depends on the rf evaporation frequency are measured. The evaporation field is applied to the atoms trapped in the magnetic

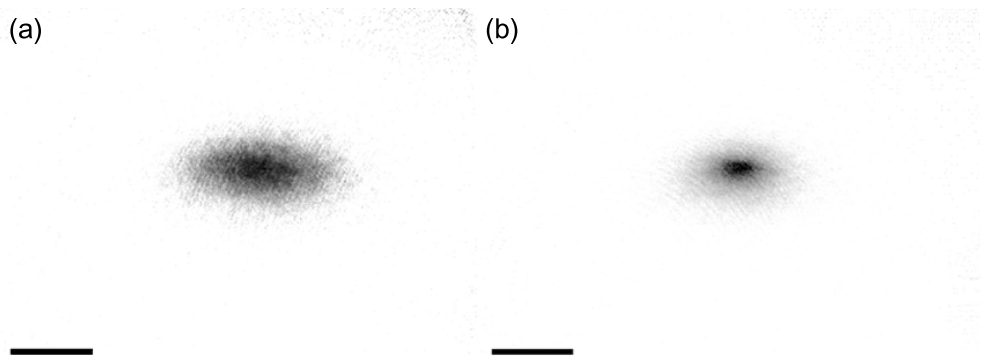

Figure 4.21: A sample image of the rf evaporative cooled atoms. (a) Atoms in a magnetic quadrupole trap (b) evaporative cooled atoms

spherical quadrupole potentials during 3 seconds.

The size of atomic cloud in a magnetic trap is depends on the geometry of the magnetic field and the frequency of the rf evaporation field, especially in the magnetic spherical quadrupole potential the size is changed linearly by the rf evaporation frequency because of the linear shape of the potential. Recall the equation of the Zeeman shift(Eq.4.9) and the magnetic potential(Eq.2.32), the resonance frequency is exactly proportional to the distance from the center. The Fig.4.6 (a) shows the result of the size changes depends on the rf frequency. The solid line is the calculated size versus the transition frequency from $m_F = -1$ to $m_F = +1$ in the magnetic trap. The difference between the calculation and the experimental result at the high frequency is the effects of the rf power broadening that is broadening of atomic linewidth by a rf field.

The Fig.4.6 (b) represent the temperature of the atomic cloud. The temperature is obtained by the size of the atoms that is mentioned at . The temperature is also changed linearly with the rf evaporation frequency.

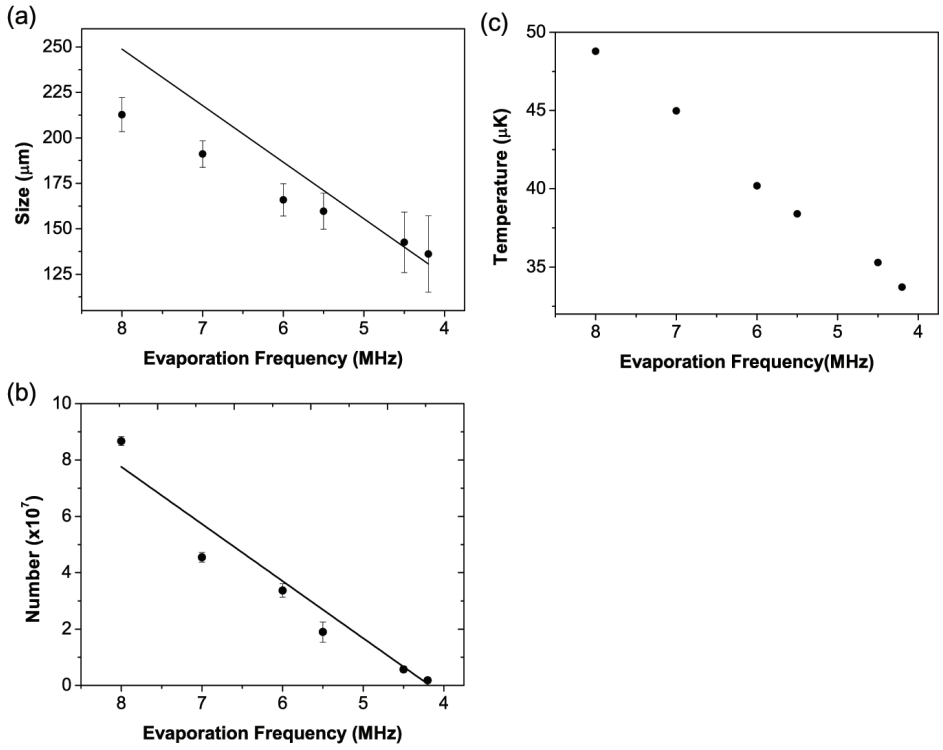

Figure 4.22: The properties of atoms in a magnetic quadrupole trap after applying rf field 3 seconds. The size(a), number(b) and temperature(c) are change linearly with the rf frequency. The dot is experimental result and the solid line is calculation from the zeeman shift. The difference between experimental result and the calculation above 7 MHz in (a) is due to the rf power broadening.

By the evaporative cooling, the phase space density(PSD) is varying with the evaporation frequency. The PSD is calculated by the relation,

$$\rho = n\lambda_T^3 \tag{4.10}$$

where, n is the density of atoms and the de-Broglie wave length $\lambda_T^3 = (\frac{2\pi\hbar}{mk_BT})^{1/2}$. The PSD is increased with lowering the trap depth by rf field but below a freqeucny(in the experiment, the frequency is $6MHz$) the majorana spin flip loss rate is sufficiently increased, the PSD is dcreased(Fig.4.6). In the magnetic quadrupole trap, it is impossible to make a Bose-Einstein condensation.

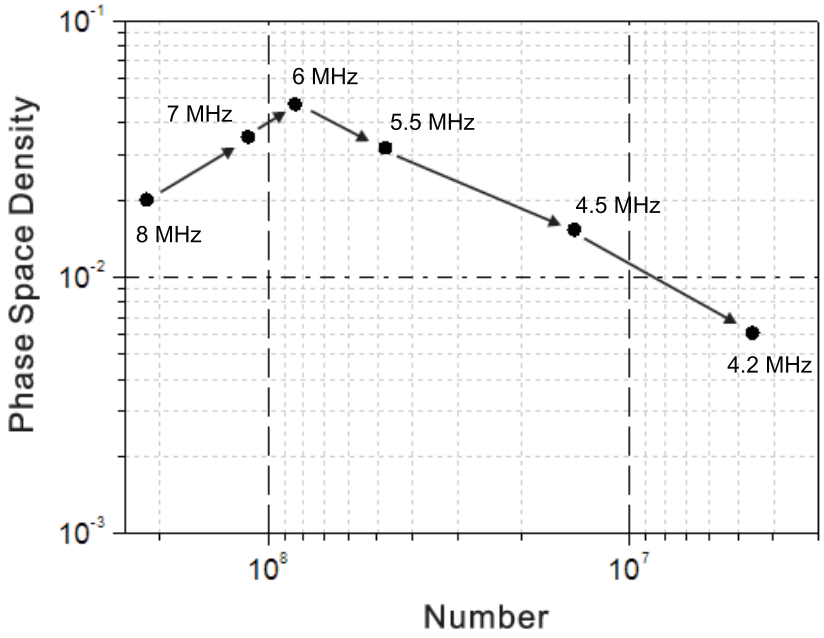

Figure 4.23: Phase space density of rf-evaporative cooled atoms in a magnetic quadrupole trap. The evaporation frequency are $8, 7, 6, 5.5, 4.5, 4.2 MHz$ respectively from left point. The maximum psd is when the rf frequency is $6 MHz$ and the psd is decreased due to the spin flip rate in the zero magnetic filed near the trap center.

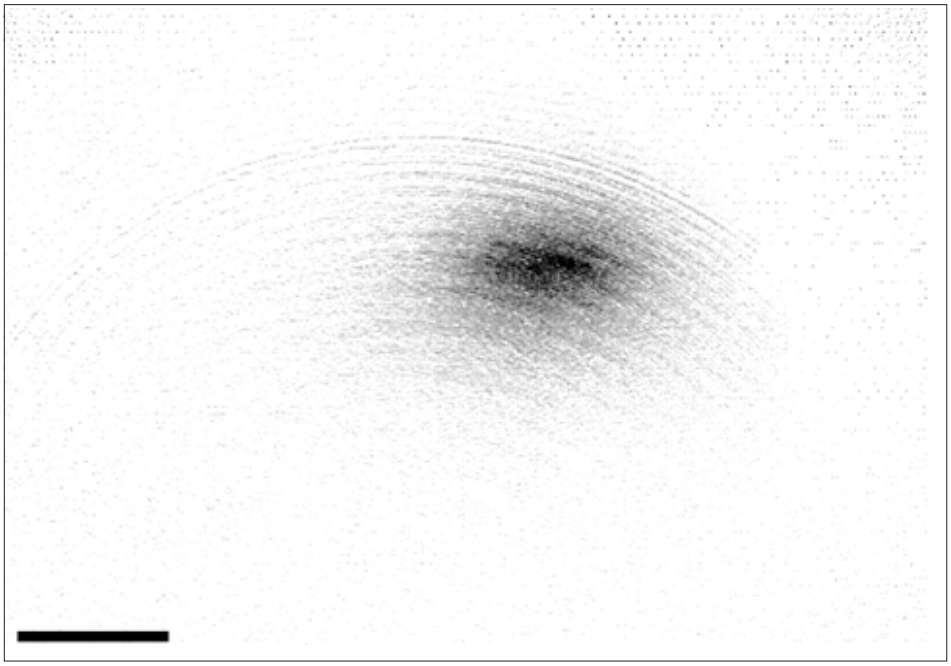

Figure 4.24: An typical image of atoms in a TOP trap after $1s$ holding. The magnetic gradient is $200G/cm$, bias field is $1.5G$ and the number of atoms is 1×10^7. The scale bar is 500 μm.

4.7 Time-averaged Orbiting Potential(TOP) Trap

The first try to overcome the loss of the majorana spin flip is instituting the time-averaged orbiting potential(TOP) trap. The TOP trap is consisted of the magnetic quadrupole field and the rotating bias field. The atoms are trapped by TOP trap after rf evaporative cooled for more efficient loading rate. An image of the trapped atoms in a TOP trap is shown at Fig.4.7.

The TOP trap has a matching condition to capture the atoms with maximum efficiency. The mode matching condition requires two conditions to be fulfilled;

1. The trap must be deep and large enough to trap most of the cooled atoms. The radius of the locus of $B = 0$ must be larger than the atomic cloud for preventing loss due to the spin flip. The radius called $'$circle of death$'$ is given by $r_0 = B_t/B_q^{'}$.

2. When the atoms are transferred to the TOP trap, there is density loss caused by the expansion or the excitation of oscillation. Thus the trap frequency of the TOP trap must be matched to the characteristic frequency of the atoms in the former trap potential.

For the TOP trap the matching condition is given by

$$\frac{B_q^{'2}}{B_t} = \frac{2k_B T}{\mu_B r^2} \tag{4.11}$$

where T and r are the temperature and size before TOP trap loading. When the matching condition is fulfilled, the number and the density of atoms in the TOP trap are preserved.

The atoms in the TOP trap is also evaporated by radio frequency to lower the temperature. However achieving Bose-Einstein condensates is failed finally. The typical image of evaporation is shown at Fig.4.7. After evaporation, the atoms are expected to decrease its size and the temperature, but the results are not matched the expectation. Only the atomic density was decreased and the size or temperature was not changed. The undesired result is estimated that there are unexpected noise in the TOP bias field.

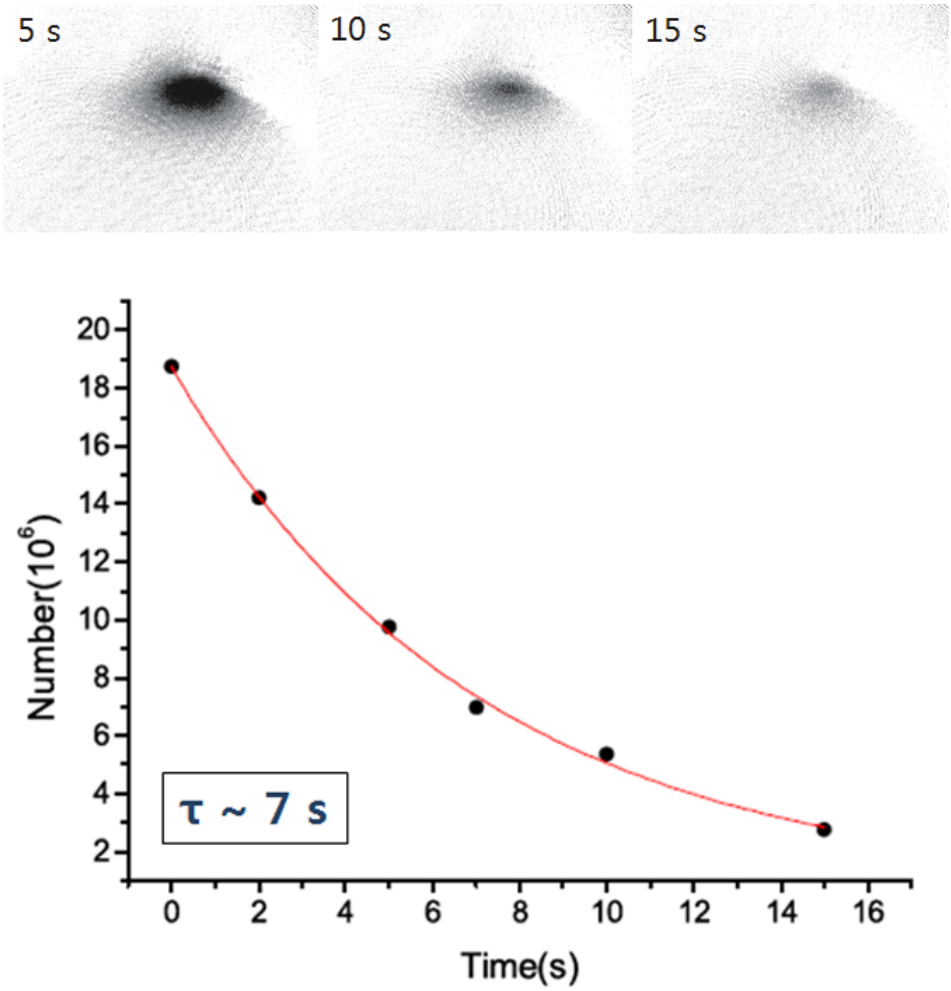

Figure 4.25: The life-time of atoms in a Top Trap. The absorption images are atoms in the TOP trap after 5 s, 10 s and 15 s. The obtained atom number in a TOP trap fitted as a exponential curve. The lifetime of atoms in a TOP trap is about 7 seconds.

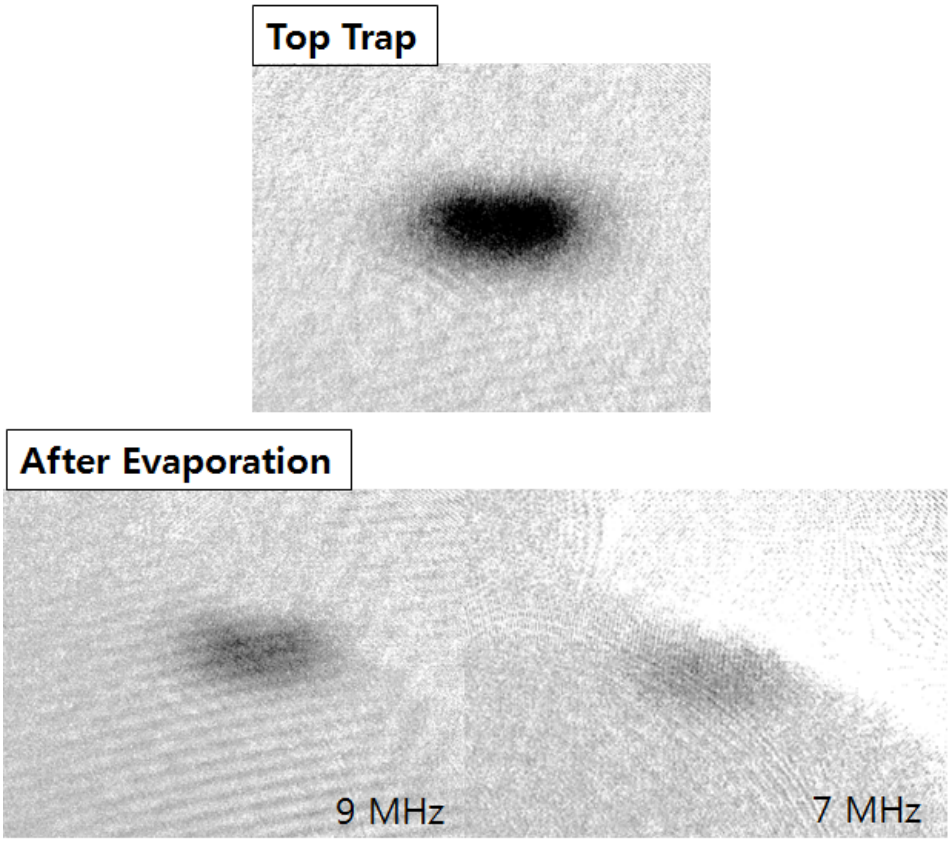

Figure 4.26: Typical image of the atoms in the TOP trap after rf evaporative cooling. (a) Image of atoms in a TOP trap (b),(c) Image of atoms after evaporation with 9 MHz and 7 Mhz respectively. The size of atoms does not changed but the intensity of atoms are decreased only.

4.8 Hybrid Trap

The hybrid trap is one of the easy way to construct a potential with magnetic spherical quadrupole trap [99] [100]. The hybrid trap is consisted of the magnetic quadrupole field and a optical dipole trap. The neutral atoms could be trapped by an optical dipole potential [101] or crossed dipole potential [76], the hybrid trap can be formed by weaker laser power than ODT only. There are two type of trapping method using optical potential and magnetic spherical quadrupole potential both. One is using blue detuned laser to block the hole near the center of the magnetic quadrupole potential and the another is using red detuned laser to trap the atoms near the center. An schematic diagram of the two methods are shown at Fig.4.8.

A 850 nm and 150 mW diode laser is used for optical dipole trap(ODT) laser. The intensity of ODT laser is controlled by an AOM and the laser passes through an optical fiber for a gaussian profile. The optical fiber and the focusing lens of ODT are attached at a xyz-translator for micro-controlling the position.

For the alignment of focal point of ODT, the ODT laser and the probe laser share the same view port of the 2nd glass chamber and the alignment of the ODT laser and the probe laser is shown at Fig.4.8. The imaging system is fitted of the location of the trapped atoms and the focal point of the ODT laser must be the center of the atoms, the laser is focused at the surface of the CCD through the imaging system. However, the intensity of the ODT laser is so high to saturate the CCD camera, it is impossible to take images of the atoms. For

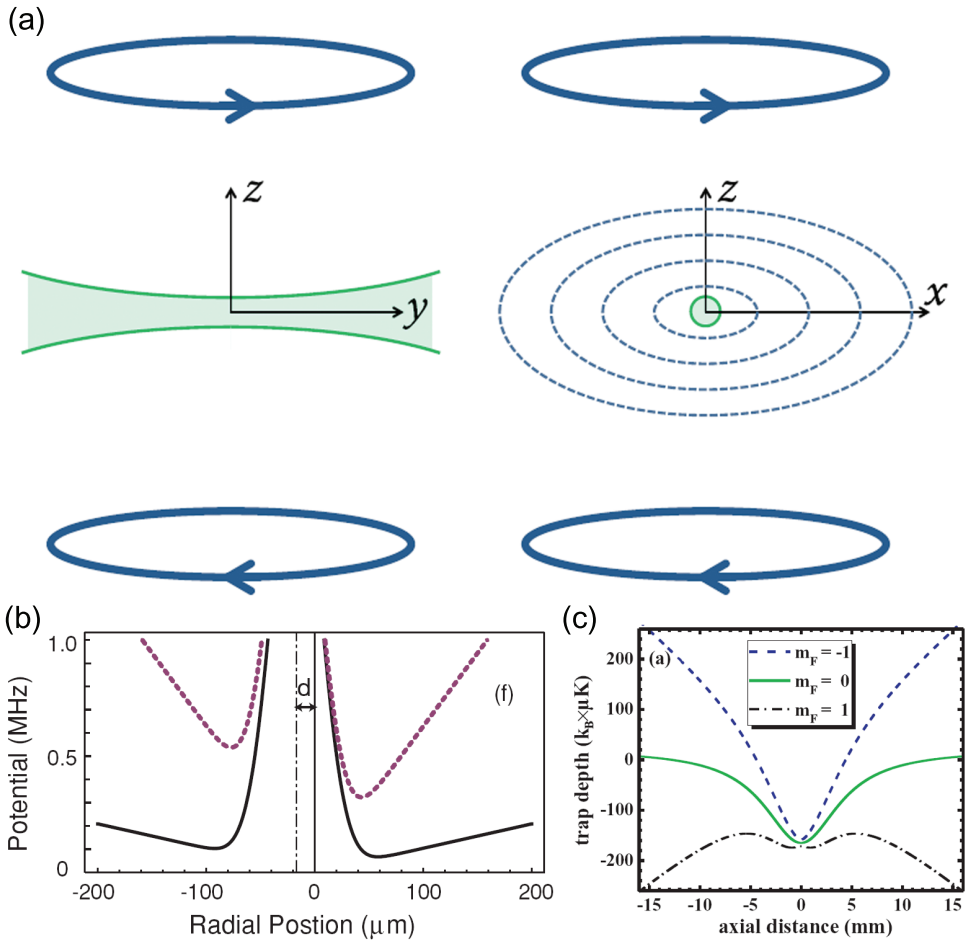

Figure 4.27: (a) The hybrid trap is consisted of a pair of AH coil and a optical dipole trap. A potential diagram of (b) optical plug beam and magnetic quadrupole trap [102] and (c) hybrid trap [103]

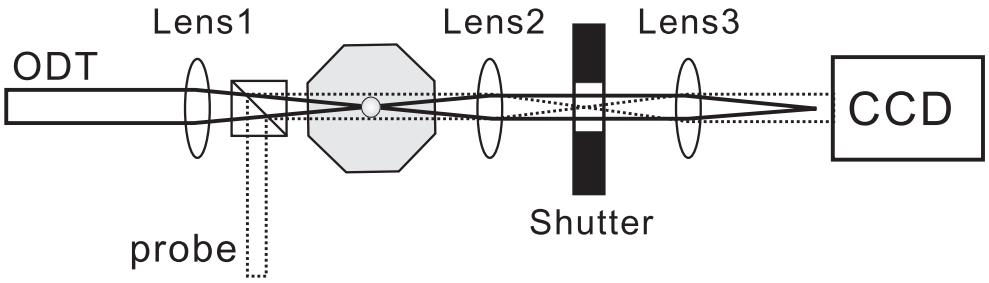

Figure 4.28: The align of optical dipole trap and probe laser.

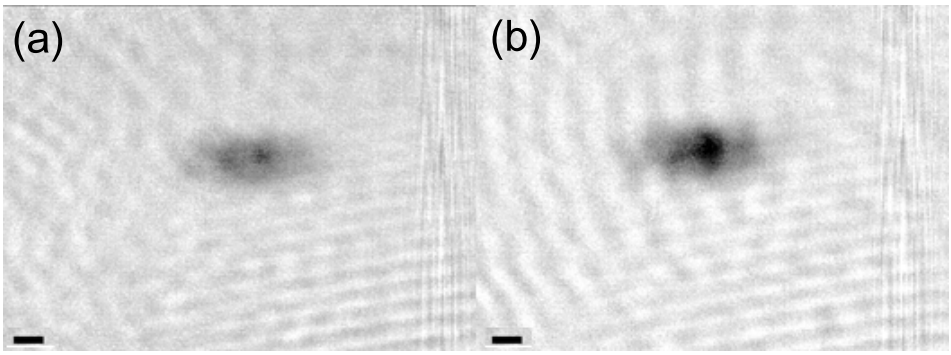

Figure 4.29: Compare (a)An image of atoms in a magnetic spherical quadrupole trap after $2MHz$ rf evaporation. The scale bar is $100\mu m$. (b) The image of trapped atoms in a hybrid trap. The trap parameters are same with (a) except the optical dipole trap.

that reason, a mechanical shutter is installed at the center of the two imaging lens.

The ODT laser is switched on after rf-evaporation in the magnetic spherical quadrupole trap. The temperature of the atoms is usually below 10 μK after the evaporation, the depth of ODT potential must be deeper than the temperature. In the experiment the beam waist is 18 μm and the power is 15 mW, the trap depth is 13 μK. An image of trapped 1×10^5 atoms in the hybrid trap is shown at Fig.4.8.

But the life time and stability of the trapped atoms in the hybrid trap is not enough for more progress. The atom loss in the hybrid trap could be explained by the laser intensity fluctuation, beam-pointing fluctuations and the quality problem of glass chamber view-port.

The heating time t_{heat} for the exponential growth of the energy of the optically trapped atoms is given by

$$\frac{1}{t_{heat}} = \pi^2 \nu_{tr}^2 S_\epsilon(2\nu_{tr}) \tag{4.12}$$

where, ν_{tr} is the trapping frequency and $S(\nu)$ is the power spectrum of the fractional magnetic field noise [104].

$$S(\omega) \equiv \frac{2}{\pi} \int_0^\infty d\tau cos(\omega t) < \epsilon(t)\epsilon(t+\tau) > \tag{4.13}$$

An estimate for $S(\omega)$ is given by $\epsilon^2/\triangle\omega$ where ϵ is the rms fractional fluctuations of the magnetic field in a bandwidth of $\triangle\omega$ [46]. And the heating time due to the beam-pointing fluctuations is given by

$$\frac{1}{t_{heat}} = \pi^2 \omega_{tr}^2 \frac{S(\omega_{tr})}{< x^2 >}. \tag{4.14}$$

The laser intensity fluctuation is less than 1 % and the heating time due to the fluctuation level is about 100 s. The instability of beam pointing due to the vibration of the xyz-stage and optics is one of the main problem of short life time in the hybrid trap. Even though fixing all the mount of the optics and the xyz-stage, there are some vibrations of the ODT laser sometimes when the

focal point is observed by the image CCD. The maximum rms variance of the motion of the ODT focal point is $1.7\mu m$ in the experiment, by the equation 4.14 the energy doubling time is $1.23s$.

The view-port of the 2nd glass chamber acts as a lens and a speckle. A incident parallel laser beam pass the 2nd glass chamber, it diverge with a angle of 0.3 degree. The lensing effect make it hard to locate the focal point of dipole trap at correct position. And also the irregular flatness of the glass gives partial deformation to the beam distribution. The irregular beam distribution is supposed to be a cause of a hole of the longitudinal confinement. By that reasons, it is needed to fix the optics of optical dipole trap perfectly and to change the glass chamber has optical flat view-port.

Chapter 5

Conclusion

The ^{87}Rb atoms are trapped in the magneto optical trap(MOT), the magnetic spherical quadrupole trap, the time-averaged orbiting potential trap and the hybrid trap. The number and temperature of atoms in the each traps are shown at Table 5.

And A new type excitation is observed in a magnetic trap induced short time compressed-MOT in the process to lower the temperature. The oscillation frequency is expected to be a measurement of trap frequency or magnetic field gradient.

Trap	Number	Temperature
MOT	Max. 5×10^9	few hundred μK
Quadrupole Trap	Max. 1×10^8	Loading $60\mu K$ Evaporation $30\mu K$
TOP Trap	Max. 1×10^7	Loading $20\mu K$
Hybrid Trap	Max. 1×10^5	Loading $10\mu K$

Table 5.1: The number and temperature of atoms

In the magnetic spherical quadrupole trap, 1×10^8 atoms are loaded and the temperature is lowered $30\mu K$ by rf-evaporative cooling. The lifetime is 26 seconds that are the evidence of good vacuum pressure and stability of magnetic trap. However it is not suited for more cooling because of majorana spin flip.

In the TOP trap, 1×10^7 atoms are trapped. For lowering temperature efficiently, atoms cooled by rf evaporation in a magnetic quadrupole trap are transferred to TOP trap. The evaporative cooling in a TOP trap decrease the density of atoms rather than lowering temperature or decreasing the phase space density. Thus the Bose-Einstein condensation is not created.

The hybrid type trap is also tried to trap ultra cold atoms. The hybrid trap is consisted of magnetic quadrupole field and a optical dipole potential. 1×10^5 atoms are trapped in a hybrid trap, the life time is not enough to lower temperature by evaporation. These experimental procedures and results are the further step to closer the Bose-Einstein condensation and the study of physics in atomic systems.

Chapter 6

Appendix

6.1 Analysis Program

The atomic properties are obtained by Gaussian fitting using analysis programs. The main analysis program is coded by the $'mathmetica'$. The analysis mathmetica program is divided five parts ;

1. Define the experiment parameters
2. Open data file and plot the image
3. Crop the interest area
4. Fitting the image as a Gaussian distribution
5. Obtaining the properties

A sample mathmetica analysis program is shown as follow.

```
Quit[]

Off[General::spell];

SetDirectory["G:\\Ph.D\\20110307"]

G:\Ph.D\20110307

(* Parameter Setting *)
m = 1.443160648 * 10^-25 ; (* Atomic mass of 87Rubidium *)
μB = 9.27400915 * 10^-24; (* Bohr magneton *)
kB = 1.3806504 * 10^-23;(*Boltzmann's constant*)
Γ = 2 π * 6.0666 * 10^6 ; (* Natural linewidth of 87Rb *)

b = 0.15; (* magnetic field grdient [T/m] unit *)
s0 = 0.05; (*s0=I/Is where Is=1.66932 mW/cm^2 *)
δ = 0 * Γ ; (* Detuning*)


(* Scattering Crosssection*)
σ = 1.36 × 10^-9 × 10^-4 × 1 / (1 + s0 + 4 (δ / Γ)^2) ;
(* scattering crosssection for equal population : unit=[m^2] *)
σ2 = 1.53 × 10^-9 × 10^-4 × 1 / (1 + s0 + 4 (δ / Γ)^2) ;
(* Scattering cross section for pumped population ?? *)
magnification = 200 / 75;
pixelSize = 6 × 10^-6 / magnification

9 / 4000000

infile = ReadList["24img2.txt", Number, RecordLists -> True];
```

```
ArrayPlot[infile, ColorFunction → GrayLevel]
Dimensions[infile]
```

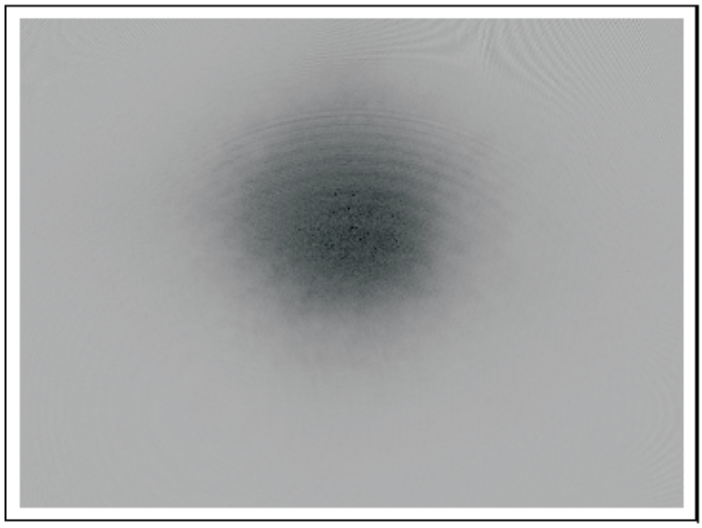

```
{1024, 1392}
```

```
rmin = 001;
rmax = 1000;
zmin = 151;
zmax = 1300;

data = infile[[rmin ;; rmax, zmin ;; zmax]];
```

```
ArrayPlot[data, ColorFunction → Hue]
```

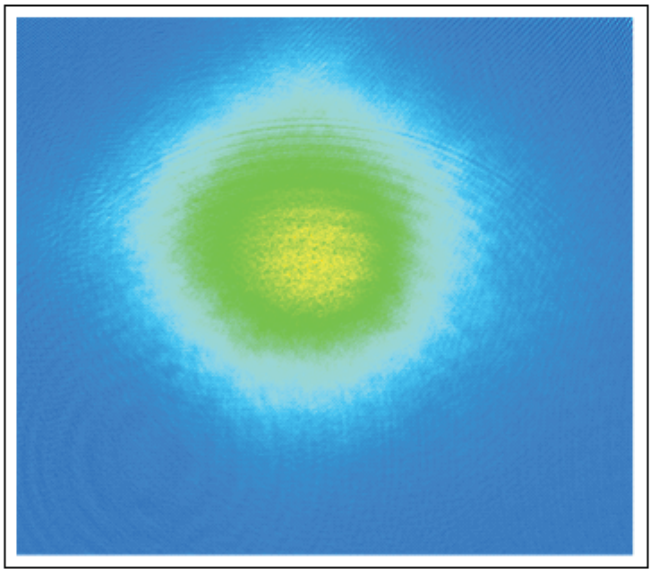

```
dim = Dimensions[data]
```

```
{1000, 1150}
```

```
Min[data]
```

```
-7.146
```

```
Position[data, Min[data]]
```

```
{{452, 570}}
```

```
bb = ListPlot[data[[500]], PlotRange → All];
aa = ListPlot[data[[All, 500]], PlotRange → All];
Gaussianfit[n0_, r0_, r_, rcenter_, bg_] :=
 bg - √π * (σ / pixelSize^2) * n0 Exp[-(r - rcenter)^2 / r0^2]
Gaussianfit[n0_, z0_, z_, zcenter_, bg_] :=
 bg - √π * (σ / pixelSize^2) * n0 Exp[-(z - zcenter)^2 / z0^2]
fitdataR = FindFit[data[[All, 500]], Gaussianfit[n0, r0, r, rcenter, bg],
   {{n0, 1}, {r0, 100}, {rcenter, 570}, {bg, 0}}, r];
fitdataZ = FindFit[data[[500]], Gaussianfit[n0, z0, z, zcenter, bg],
   {{n0, 1}, {z0, 100}, {zcenter, 500}, {bg, 0}}, z];
aaa = Plot[Gaussianfit[n0, r0, r, rcenter, bg] /. fitdataR,
   {r, 0, 1000}, PlotStyle → {Green, Thickness[0.01]}];
bbb = Plot[Gaussianfit[n0, z0, z, zcenter, bg] /. fitdataZ,
   {z, 0, 1150}, PlotStyle → {Purple, Thickness[0.01]}];

Show[aa, aaa]
Show[bb, bbb]
```

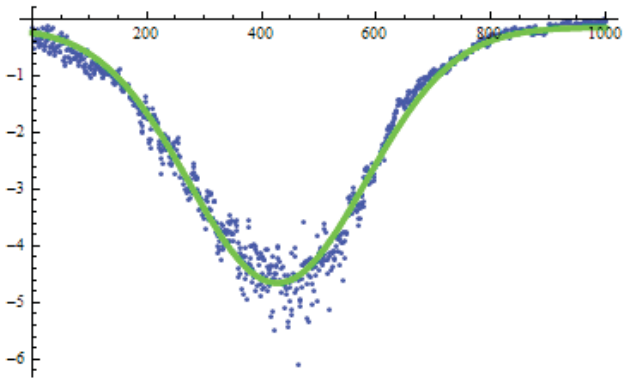

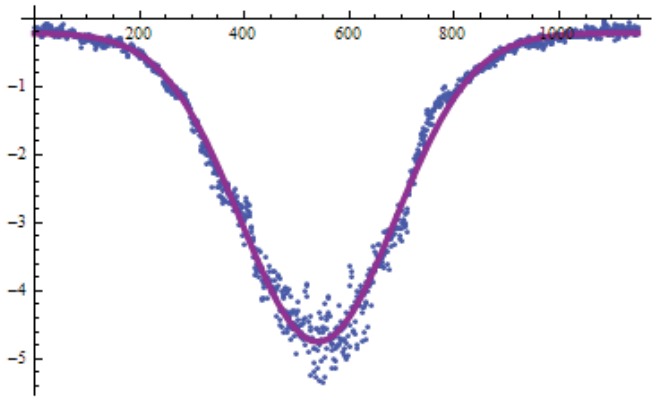


```
Gaussianfit[n0_, r0_, z0_, r_, z_ , rcenter_, zcenter_, bg_] :=
 bg - √π * (σ / pixelSize^2) * n0 * r0 *
   Exp[-(r - rcenter)^2 / r0^2 - (z - zcenter)^2 / z0^2]
```

```
Data2D = Flatten[Table[{i, j, data[[i, j]]}, {i, 1, dim[[1]]},
    {j, 1, dim[[2]]}], 1];
```

```
Data2D[[2]]
```

```
{1, 2, 0.316}
```

```
fitdata =
 FindFit[Data2D, Gaussianfit[n0, r0, z0, r, z, rcenter, zcenter, bg],
  {{n0, 0.1}, {r0, 100}, {z0, 100}, {rcenter, 500}, {zcenter, 600},
   {bg, 0}}, {r, z}]
```

```
{n0 → 0.111492, r0 → 150.324, z0 → 227.006,
 rcenter → 483.716, zcenter → 611.721, bg → -0.0659514}
```

```
DensityPlot[-Gaussianfit[n0, r0, z0, r, z, rcenter, zcenter, bg] /.
  fitdata, {r, 0, 1000}, {z, 0, 1150}, Mesh → False,
 ColorFunction → "BlueGreenYellow", PlotPoints → 100, PlotRange → All]
```

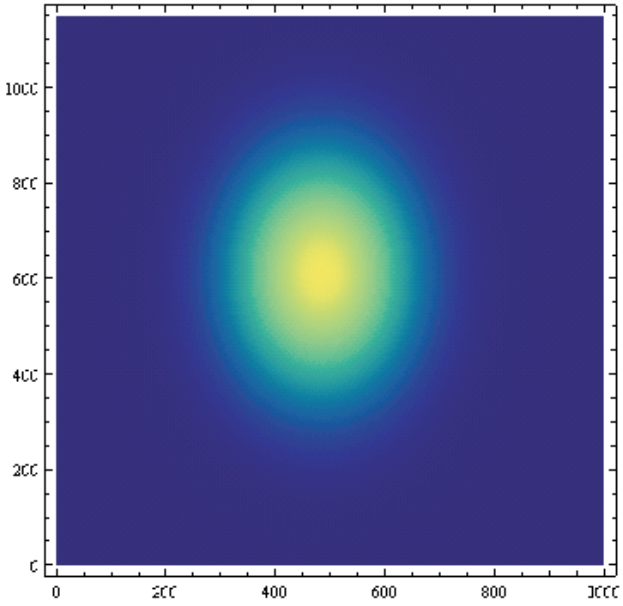


```
fitdata
```

```
{n0 → 0.111492, r0 → 150.324, z0 → 227.006,
 rcenter → 483.716, zcenter → 611.721, bg → -0.0659514}
```

```
n0 /. fitdata
```

```
0.111492
```

```
Ntot = n0 Pi^(3/2) r0^2 z0 /. fitdata
```

3.18463×10^{6}

```
Plot3D[-Gaussianfit[n0, r0, z0, r, z, rcenter, zcenter, bg] /. fitdata,
 {r, 0, 1000}, {z, 0, 1150}, Mesh → False, ColorFunction → "Rainbow",
 PlotPoints → 100, PlotRange → All]
```

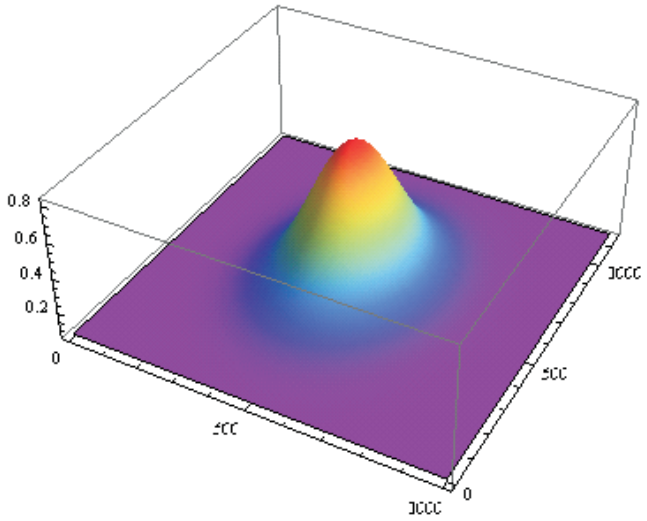


```
ρz = r0 6 10^-4 /. fitdata (* [cm] *)
ρr = z0 6 10^-4 /. fitdata (* [cm] *)
num = 2 Ntot / (3 π ρr^2 ρz) (* [number/cm^3] *)
```

0.0901942

0.136203

4.0389×10^{8}

6.2 Rubidium 87 Data

Atomic Number	Z	37
Total Necleons	Z + N	87
Relative Natural Abundance	$\eta(^{87}Rb)$	
Nuclear Lifetime	τ_n	$4.88 \times 10^{10}\ yr$
Atomic Mass	m	$1.44316060(11) \times 10^{-25}\ kg$
Density at $25°C$	ρ_m	$1.53\ g/cm^3$
Melting Point	T_M	$39.31\ °C$
Boiling Point	T_B	$688\ °C$
Vapor Pressure at $25°C$	P_v	$3.0 \times 10^{-7}\ torr$
Nuclear Spin	I	3/2

Table 6.1: ^{87}Rb Physical Properties

Frequency	ω_0	$2\pi \cdot 384.2279818773(55)\ THz$
Wavelength(Vacuum)	λ	$780.246291629(11)\ nm$
Wavelength(Air)	λ_{air}	$780.03708\ nm$
Wave Number(Vacuum)	$k_L/2\pi$	$12816.46591247(18)\ cm^{-1}$
Lifetime	τ	$26.24(4)\ ns$
Decay Rate/ Natural Line Width(FWHM)	Γ	$36.11(6) \times 10^6\ s^{-1}$ $2\pi \cdot 6.065(9)\ MHz$
Recoil Velocity	v_r	$5.8845\ mm/s$
Recoil Energy	ω_r	$2\pi \cdot 3.7709\ kHz$
Recoil Temperature	T_r	$361.95\ nK$
Doppler Shift($v_{atom} = v_r$)	$\triangle\ \omega_d$	$2\pi \cdot 7.5418\ kHz$
Doppler Temperature	T_D	$146\mu\ K$

Table 6.2: $^{87}RbD2(5^2S_{1/2} \rightarrow 5^2P_{3/2})$ Transition optical properties

Bibliography

[1] P. Kapitza, Nature **141**, (1938).

[2] J. Bardeen, L. N. Cooper, and J. R. Schrieffer, Phys. Rev. **108**, 1175 (1957).

[3] E. article, Nature Physics **6**, 713 (2010).

[4] F. Reif, *Fundamentals of statistical and thermal physics* (McGraw-Hill international editions, Singapore, 1985).

[5] A. V. Martynov, Chemical and Petroleum Engineering **12**, (1976).

[6] W. Cullen, *Of the Cold Produced by Evaporating Fluids and of Some Other Means of Producing Cold* (PUBLISHER, ADDRESS, YEAR).

[7] A. M. Arkharov, Chemical and Petroleum Engineering **31**, (1995).

[8] W. M. Haynes, *CRC Handbook of Chemistry and Physics, 93rd Edition* (CRC press, Boulder, USA, 2012).

[9] S. B. Bose, Z. Phys. **26**, (1924).

[10] A. Einstein, Physikalisch-mathematische Klasse 261 (1924).

[11] F. London, Nature **141**, (1938).

[12] F. London, Phys. Rev. **54**, (1938).

[13] P. D. Lett *et al.*, PRL **61**, (1998).

[14] W. D. Phillips, Rev. Mod. Phys. **70**, 721 (1998).

[15] M. H. Anderson *et al.*, Science **269**, 198 (1995).

[16] K. B. Davis *et al.*, Phys. Rev. Lett. **75**, 3969 (1995).

[17] C. C. Bradley, C. A. Sackett, J. J. Tollett, and R. G. Hulet, Phys. Rev. Lett. **75**, 1687 (1995).

[18] G. Modugno *et al.*, Science **294**, 1320 (2001).

[19] T. Weber *et al.*, Science **299**, 232 (2003).

[20] S. L. Cornish *et al.*, Phys. Rev. Lett. **85**, 1795 (2000).

[21] D. G. Fried *et al.*, Phys. Rev. Lett. **81**, 3811 (1998).

[22] A. Robert *et al.*, Science **292**, 461 (2001).

[23] F. P. D. Santos *et al.*, Phys. Rev. Lett. **86**, 3459 (2001).

[24] Y. Takasu *et al.*, Phys. Rev. Lett. **91**, (2003).

[25] D. S. Durfee and W. Ketterle, Optics Express **2**, (1998).

[26] Y. Kim, D. Yum, H. R. Hoh, and W. Jhe, Opt. Comm. **284**, 2876 (2011).

[27] M. S. Heo *et al.*, Phys. Rev. A **75**, 023409 (2007).

[28] H. Fechbach, Annals of Physics **5**, 357 (1958).

[29] S. Inouye *et al.*, Nature **392**, 151 (1998).

[30] I. Bloch *et al.*, Phys. Rev. A **64**, 021402 (2001).

[31] S. B. Papp and C. E. Wieman, Phys. Rev. Lett. **97**, 180404 (2006).

[32] M. Haas *et al.*, New J. Phys. **9**, 147 (2007).

[33] J. Herbig *et al.*, Science **30**, (2003).

[34] C. A. Regal, C. Ticknor, J. L. Bohn, and D. S. Jin, Nature **424**, 47 (2003).

[35] M. W. Zwierlein *et al.*, Phys. Rev. Lett. **91**, 250401 (2003).

[36] T. Bourdel *et al.*, Phys. Rev. Lett. **93**, 050401 (2004).

[37] M. P. A. Fisher, P. B. Weichman, G. Grinstein, and D. S. Fisher, Phys. Rev. B **40**, 546 (1989).

[38] D. Jaksch *et al.*, Phys. Rev. Lett **81**, 3108 (1998).

[39] M. Griner *et al.*, Nature **415**, 39 (2002).

[40] F. S. Cataliotti *et al.*, Science **293**, 843 (2001).

[41] O. Morsch *et al.*, Phys. Rev. Lett. **87**, (2001).

[42] W. K. Hensinger *et al.*, Nature **412**, 52 (2001).

[43] D. A. Huse and E. D. Siggia, J. Low. Temp. Phys. **46**, (1982).

[44] D. V. Schroeder, *Thermal Physics* (Addison Wesley Longman, New York, 1999).

[45] V. Bagnato, D. E. Pritchard, and D. Kleppner, Phys. Rev. A **35**, (1987).

[46] W. Ketterle, D. S. Durfee, and D. M. Stemper-Kurn, arXiv:cond-mat/9904034v2 (1999).

[47] P. Ehrenfest, Zeit. f. Phys. **45**, 455 (1927).

[48] E. Raab *et al.*, Phys. Rev. Lett. **59**, 2631 (1982).

[49] C. Monroe, W. Swann, H. Robinson, and C. Wieman, Phys. Rev. Lett. **65**, 1571 (1990).

[50] H. J. Metcalf and P. van der Straten, *Laser cooling and trapping* (Springer, New York, 1999).

[51] D. Sesko *et al.*, Phys. Rev. Lett **63**, (1989).

[52] W. Gerlach and O. Stern, Zeitschrift f*ü*r Physik a Hadrons and Nuclei **9**, (1922).

[53] W. Wing, Prog. Quant. Elect. **8**, 181 (1984).

[54] E. Majorana, Nuovo Cim. N. S. **9**, 43 (1932).

[55] A. Migdall *et al.*, Phys. Rev. Lett. **54**, 2596 (1985).

[56] T. Bergeman, G. Erez, and H. Metcalf, Phys. Rev. A **35**, 1535 (1987).

[57] D. M. Brink and C. V. Sukumar, Phy. Rev. A **74**, 1 (2006).

[58] M. Inguscio, Proceedings of Science (2006).

[59] M. O. Mewew *et al.*, Phys. Rev. Lett. **77**, 416 (1996).

[60] W. Petrich, M. H. Anderson, J. R. Ensher, and E. A. Cornell, PRL **74**, 3352 (1995).

[61] C. C. Bradley, C. A. Sackett, and R. G. Hulet, Phys. Rev. A **58**, 985 (1997).

[62] T. Esslinger, I. Bloch, and T. W. Hansch, Phys. Rev. A **58**, R2664 (1998).

[63] J. Soding *et al.*, Appl. Phys. B **69**, 257 (1999).

[64] T. Bergeman, G. Erez, and H. Metcalf, Phys. Rev. Lett **35**, 1535 (1987).

[65] C. R. Monroe *et al.*, Phys. Rev. Lett. **70**, 414 (1993).

[66] W. Ketterle and N. J. Druten, Adv. At. Mol. Opt. Phys. **37**, 181 (1996).

[67] H. F. Hess, Phys. Rev. B **34**, 3476 (1986).

[68] K. J. Kügler, K. Moritz, W. Paul, and U. Trinks, Nuc. Instrum. Methods Phys. Res. **228**, 240 (1985).

[69] H. Hess *et al.*, Phys. Rev. Lett. **59**, 672 (1987).

[70] C. S. Adams *et al.*, Phys. Rev. Lett. **74**, 3577 (1995).

[71] N. Masuhara *et al.*, Phys. Rev. Lett. **61**, 935 (1988).

[72] A. G. Martin *et al.*, Phys. Rev. Lett. **61**, 2431 (1988).

[73] D. E. Pritchard, K. Helmerson, and A. G. Martin, At. Phys. **11**, 179 (1989).

[74] M. Yamashita *et al.*, Phys. Rev. A **67**, 023601 (2003).

[75] B. E. A. Saleh and M. C. Teich, *Fundamentals of photonics* (John Wiley and Sons, Inc., New York, 1991).

[76] C. S. Adams *et al.*, Phys. Rev. Lett. **74**, 3577 (1995).

[77] R. Grimm, M. Weidemuller, and Y. B. Ovchinnikov, Adv. At. Mol. Opt. Phys. **42**, 95 (2000).

[78] R. Ozeri, L. Khaykovich, and N. Davidson, Phys. Rev. A **59**, R1750 (1999).

[79] N. Friedman, L. Khaykovich, R. Ozeri, and N. Davidson, Phys. Rev. A **61**, 031403 (2000).

[80] J. P. Gordon and A. Ashkin, Phys. Rev. A **21**, 1606 (1980).

[81] J. Dalibard and C. Cohen-Tannoudji, J. Opt. Soc. Am. B **2**, 1707 (1985).

[82] G. K. Woodgate, *Elementary atomic structure* (Mcgraw-hill, London, 1970).

[83] C. Wieman, G. Flowers, and S. Gilbert, Am. J. Phys. **63**, (1994).

[84] D. Yum, J. Park, W. Lee, and W. Jhe, J. Korean Phys. Soc. **60**, (2012).

[85] C. J. Myatt *et al.*, Optics Letters **21**, (1996).

[86] J. A. Kim *et al.*, Opt. Lett. **22**, 117 (1997).

[87] K. B. MacAdam, A. Steinbach, and C. Wieman, Am. J. Phys. **60**, (1992).

[88] E. A. Donley *et al.*, Rev. Sci. Instrum. **76**, 063112 (2005).

[89] H. J. Lewandowski, D. M. Harber, D. L. Whitaker, and E. A. Cornell, J Low. Temp. Phys. **132**, 309 (2003).

[90] C. J. Foot, *Atomic Physics* (Oxford, New York, 2005).

[91] V. V. Goldman, I. F. Silvera, and A. J. Leggett, Phys. Rev. B **24**, (1981).

[92] W. Petrich, M. H. Anderson, J. R. Ensher, and E. A. Cornell, J. Opt. Soc. Am. B **11**, (1994).

[93] C. G. Townsend *et al.*, Phys. Rev. A **52**, 4194 (1995).

[94] J. Dalibard and C. Cohen-Tannoudji, J. Opt. Soc. Am. B **6**, (1989).

[95] D. S. Weiss *et al.*, J. Opt. Soc. Am. B **6**, 2072 (1989).

[96] P. J. Ungar, D. S. Weiss, E. Riis, and S. Chu, J. Opt. Soc. Am. B **6**, 2058 (1989).

[97] *Optical pumping of Rubidium : Guide to the experiment Instructor's manual* (TeachSpin, Inc., ADDRESS, 2002).

[98] T. H. Bergeman *et al.*, J. Opt. Soc. Am. B **6**, (1989).

[99] Y. J. Lin *et al.*, Phys. Rev. A **79**, 063631 (2009).

[100] M. Zaiser *et al.*, Phys. Rev. A **83**, 035601 (2011).

[101] S. Chu, J. E. Bjorkholm, A. Ashkin, and A. cable, Phys. Rev. Lett **57**, 314 (1986).

[102] M. S. Heo, J. Choi, and Y. Shin, Phy. Rev. A **83**, 013622 (2011).

[103] D. S. Naik and C. Raman, Phy. Rev. A **71**, 033617 (2005).

[104] T. A. Savard, K. M. O'Hara, and J. E. Thomas, Phys. Rev. A **56**, R1095 (1997).